



## Research papers

# Predicting post-fire hydrological and erosive catchment response during rainfall events. A comparison of OpenLISEM and MOHID Land models

Marta Basso <sup>a,\*</sup>, Jantiene Baartman <sup>b</sup>, Martinho Martins <sup>a</sup>, Jacob Keizer <sup>c</sup>, Diana Vieira <sup>d</sup>

<sup>a</sup> Centre for Environmental and Marine Studies (CESAM), Department of Environment and Planning, University of Aveiro, Aveiro, Portugal

<sup>b</sup> Soil Physics and Land Management Group, Wageningen University and Research, The Netherlands

<sup>c</sup> GeoBioTec, Department of Environment and Planning, University of Aveiro, Portugal

<sup>d</sup> European Commission, Joint Research Centre (JRC), Ispra, Italy



## ARTICLE INFO

This manuscript was handled by Sally Elizabeth Thompson, Editor-in-Chief, with the assistance of Tessa Maurer, Associate Editor

## Keywords:

Rainfall-runoff

Erosion

Hydrological model

Wildfire

Catchment hydrology

## ABSTRACT

Wildfires are a source of instability for the natural water cycle in forested watersheds, endangering the water quantity and quality reaching downstream water bodies. The faster hydrological response of a burned area leads to increased runoff and transport of sediment and ash particles during and after rainfall events. Therefore, the use of an adequate spatiotemporal resolution in hydrological models is necessary to properly estimate post-fire impacts. Especially when addressing hydrological events such as flash floods and debris flows, which are highly unpredictable and are characterized by short duration and high impact outside the burned area.

This study aims to compare the ability of two hydrological models to simulate the hydrological response and sediment transport during the first year after a fire to ultimately understand which one would best serve as a post-fire hydrological predicting tool at event scale. To achieve this goal, OpenLISEM, an event-based hydrological model, and MOHID Land, a continuous model with variable timestep, were compared. Driven by several limitations identified in previous modeling exercises at this scale during the calibration phase, this work performed a parametrization through the variation in boundary conditions characterizing each event.

OpenLISEM and MOHID Land models exhibited similar capabilities in simulating runoff during the first post-fire year. However, the larger erosion input parameters required by MOHID Land increase the complexity of erosion prediction and increase equifinality. In addition, MOHID Land limited capacity to perform sensitivity and uncertainty analyses emerged as a major disadvantage, hindering the assessment of the reliability of the model's predictions. Despite its limitations for not integrating subsurface flow and base flow, OpenLISEM is the most suitable model for assessing post-fire impacts on runoff and sediment production at the event scale, because of its ease of implementation and its reduced computational requirements.

## 1. Introduction

Wildfires are a source of instability for the natural hydrological cycle of a watershed (Shakesby, 2011; Shakesby and Doerr, 2006). The consumption of vegetation leaves the soil unprotected and vulnerable to rain and wind erosion (Moody et al., 2013; Shakesby, 2011). Vegetation consumption leads to the formation of charred debris and a highly erosive layer of ash (Pereira et al., 2015), whose thickness depends on the availability of biomass and the severity of the fire. Moreover, heat-induced changes in soil properties can reduce the infiltration capacity of the first layer of soil, increasing overland flow (Keizer et al., 2008; Moody et al., 2013; Shakesby, 2011). The combination of these two

processes causes land degradation and increased sediment mobilization and ash runoff, posing a threat to the water quality of downstream waterbodies (Bladon et al., 2014; Campos et al., 2012; Emelko et al., 2011; Nunes et al., 2018a; Smith et al., 2011). The magnitude of impacts depends on different factors, mainly the soil burn severity (Keeley, 2009; Vieira et al., 2015), the post-fire weather regime (Murphy et al., 2015; Wagenbrenner et al., 2021), and pre-fire land cover.

Hydrological models are widely used for the assessment and understanding of post-fire impacts, as they allow to include the interplay of several factors (Basso et al., 2022a). However, studies integrating calibration and validation of post-fire response are scarce due to data collection limitations and limited availability of field data (Basso et al.,

\* Corresponding author.

E-mail address: [martabasso@ua.pt](mailto:martabasso@ua.pt) (M. Basso).

<https://doi.org/10.1016/j.jhydrol.2024.131258>

Received 6 June 2023; Received in revised form 10 January 2024; Accepted 10 April 2024

Available online 29 April 2024

0022-1694/© 2024 The Authors. Published by Elsevier B.V. This is an open access article under the CC BY-NC license (<http://creativecommons.org/licenses/by-nc/4.0/>).

2022a; Lopes et al., 2021), especially at catchment scale. Empirical models, in particular the revised version of the Universal Soil Loss Equation (USLE), RUSLE (Renard et al., 1991), are commonly applied to burned areas for estimating annual soil erosion at the hillslope scale (Fernández and Vega, 2016; Larsen and MacDonald, 2007; Rulli et al., 2013; Vieira et al., 2018b) driven by the simplicity of their implementation, but also due to a high input data availability worldwide (Vieira et al., 2018). Models that allow higher spatial and temporal resolution are generally applied to increase the level of detail of post-fire impact predictions. Most physical and processes-based models used to assess the impacts of wildfires on the overland flow and stream water quality are applied at monthly and daily time steps at watershed scale (Basso et al., 2022b, 2020; Havel et al., 2018; Moussoulis et al., 2015; Nunes et al., 2018b). The use of event-based models, which allow the prediction of impacts at higher temporal resolution (minutes), is less common (Canfield et al., 2005; Chen et al., 2013; Liu et al., 2021; Rengers et al., 2016; Van Eck et al., 2016; Vieira et al., 2022; Wu et al., 2021a, 2021b). Continuous models with daily or monthly time steps are often used for estimating long-term wildfire impacts, such as changes in the natural hydrological cycle of the catchment and water quality under management scenarios (Basso et al., 2022b).

Given the rapid post-fire response often leading to flash floods, debris flows and mudflows (Cannon et al., 2008; Moody et al., 2013; Neary and Gottfried, 2002), the use of continuous models at larger time steps can cause smoothing of predictions during rainfall events, due to inadequate temporal resolution that may not correctly represent the runoff peaks (Vieira et al., 2022). Since precipitation is the primary driver of post-fire responses (Moody et al., 2013), the expected increase in runoff and sediment transport is more evident during and following rainfall events. Therefore, an increase in resolution during this temporal window is expected to benefit the estimation of the magnitude and the timing of the hydrological response, especially following heavy rainstorms that could lead to destructive off-site effects. Notwithstanding, some limitations have been identified for event-based modeling, such as the inability to achieve high model performances during the validation procedure with a single parameter dataset for several events (Baartman et al., 2012; Rengers et al., 2016; Vieira et al., 2022; Wu et al., 2021a). This invalidates the capacity of an event-by-event calibration to predict future occurrences.

This study aims to assess the performance of two hydrological models in predicting the post-fire hydrological and erosive response at event scale in the first year after the fire. Based on previous post-fire hydrological model exercises at event scale (Van Eck et al., 2016; Vieira et al., 2022; Wu et al., 2021b, 2021a), this work intends to perform a calibration considering a consistency between the calibrated parameters for the events and the boundary conditions characterizing each event. To achieve such objective, OpenLISEM, an event-based hydrological and soil erosion model (De Roo et al., 1996b, 1996a), and MOHID Land (Trancoso et al., 2009), a continuous model with variable timestep, were applied and compared. The major difference between the models is considering (MOHID Land) or not (OpenLISEM) slow processes such as evapotranspiration and base flow. The specific objectives of the study were: (i) to provide a methodology that allows to obtain input hydrological parameters from event characteristics and burn severity; (ii) to compare the ability of OpenLISEM and MOHID Land to simulate hydrological response and sediment transport during the first post-fire year, and (iii) to understand which model would best serve as a tool for event-scale post-fire hydrological assessment.

## 2. Materials and methods

### 2.1. Hydrological models: OpenLISEM and MOHID Land

The Limburg Soil Erosion Model (OpenLISEM) is a process-based, spatially distributed model that simulates runoff events incorporating precipitation, interception, surface storage and infiltration into the soil,

surface runoff and channel flow (De Roo et al., 1996b, 1996a). The event-based nature of the version of the model used for this study (OpenLISEM 6.41) excludes slow processes such as evapotranspiration and base flow. Infiltration was simulated using the Green-Ampt one-layer model, while the surface flow was based on the 2D Kinematic wave equation. The channel system was not included since the water reaches the outlet flows through a short narrow intermittent stream that runs over the parent rock. Together with the hydrological process, OpenLISEM can simulate erosion and deposition processes. The amount of suspended sediments is calculated as the difference between the sum of the rain splash and the runoff detachment with the deposition. The equation considers detachment as a process dependent on the cohesion of the soil material, controlled by a dimensionless efficiency factor. This factor is found to be constant and equal to one when deposition occurs, while it is calculated from cohesion when erosion occurs. The flow detachment was simulated using the Morgan, Morgan and Finney model (Morgan, 2001) for the detachment efficiency, and the settling velocity was based on the Stokes equation for small grains, and Zanke (1977) equation for larger ones. The splash detachment in OpenLISEM is simulated using a derived equation from splash tests, where the rainfall kinetic energy is calculated using the negative exponential equation defined by van Dijk et al. (2002). OpenLISEM was already adapted at catchment scale to simulate post-fire conditions in Portugal using an event-by-event calibration process (Van Eck et al., 2016; Vieira et al., 2022; Wu et al., 2021a, 2021b).

MOHID Land is a physically-based, spatially distributed model (Trancoso et al., 2009). In comparison to OpenLISEM, MOHID Land simulates the subsurface flow and the transport of nutrients and contaminants. The infiltration is based on Richards' equation where the soil hydraulic properties are described using van Genuchten and Mualem models (Mualem, 1976; van Genuchten, 1980). The overland flow is simulated using the 2D Kinematic wave equation as in OpenLISEM. Unlike OpenLISEM, MOHID Land does not allow the exclusion of the channel system since it does not differentiate the channel network from the drainage network. To simulate the presence of the intermittent stream, all elements of the drainage network were considered of 1st order (Strahler, 1957). Erosion and deposition are a function of the shear stress, and sediments are only represented as a clay phase. Splash erosion by raindrop impact is simulated by always considering the erosion coefficients relative to clay. Unlike OpenLISEM, this process is calculated only for water columns below a critical value, above which splash erosion is not efficient or does not impact particles with sufficient strength. No other event-scale application of MOHID Land is reported in the literature. In addition, tests and calibrations of model's ability to simulate sediment transport are scarce (Brito et al., 2018).

### 2.2. Study area

The area used for this modeling work was Serra de Cima catchment (5.16 km<sup>2</sup>; 40.60915, -8.34037), located in the Caramulo mountains in the North-Central region of Portugal (Fig. 1.a). Before the wildfire, the area was covered mainly by a mosaic of eucalyptus plantations in different rotation cycles (Fig. 1.c), except for a small stand of mixed forest close to the outlet. Between August 8th and 13th 2016, a wildfire burned approximately 74 % of the catchment area. Burn severity within the Serra de Cima catchment was mapped using the difference Normalized Burn Ratio (dNBR), distinguishing three severity classes following Lutes et al., (2006): low [0.1–0.27], moderate [0.27–0.66], and high [0.66–1.3] (Fig. 1.d). The pre- and post-fire NBR maps were derived from the near-infrared (NIR) and shortwave infrared (SWIR) bands of satellite Sentinel 2 images from 19th July 2016 and 18th August 2016, having a spatial resolution of 10 m. The moderate and high dNBR severity agreed with the severities at the 9 plots installed in the field, where 6 were characterized by moderate and the remaining 3 by high burn severity. The climate of the area is classified as temperate with mean annual temperature and rainfall in the region for the last 25 years

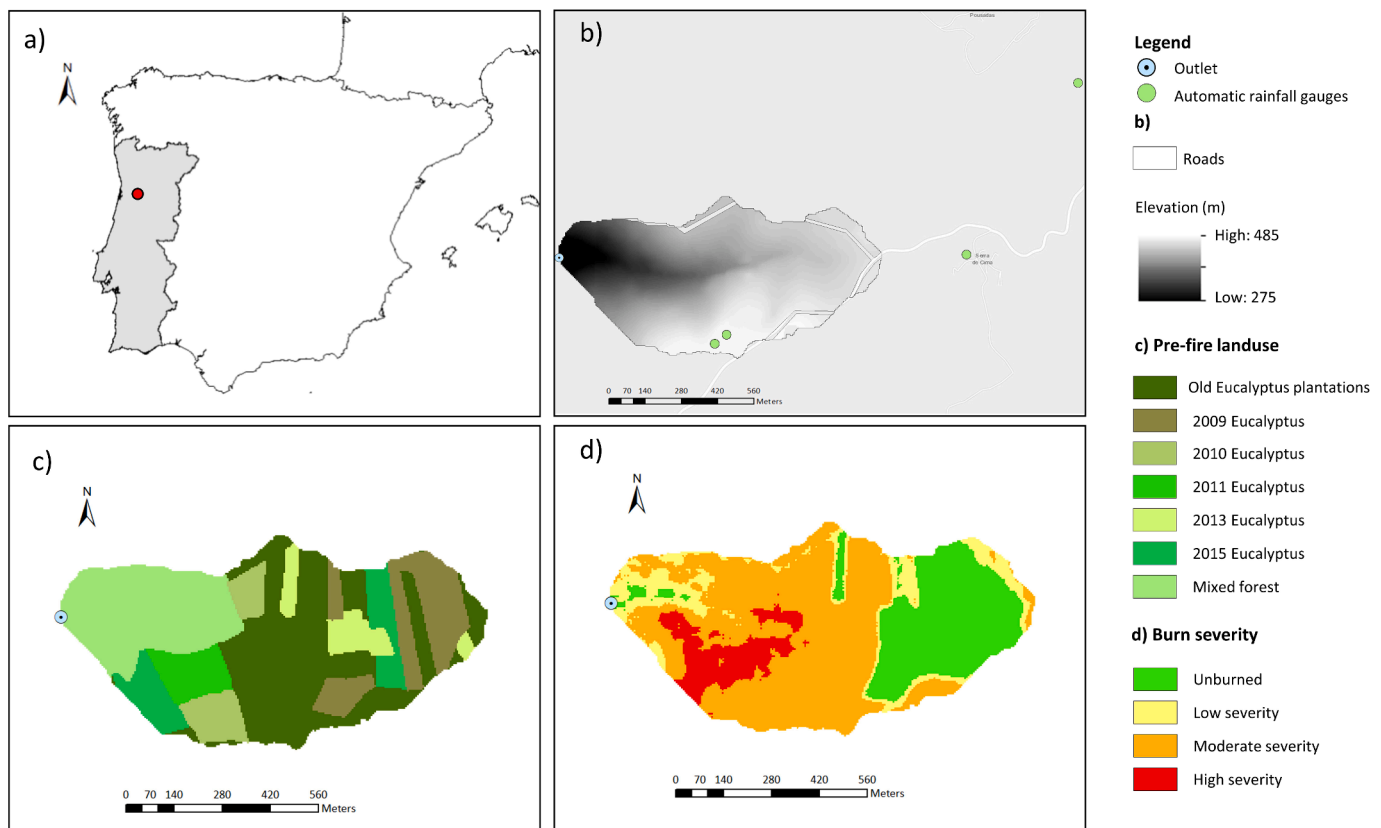


Fig. 1. (a) Study area location, (b) Digital Elevation Model (DEM) and rainfall gauges, (c) Land use in the pre-fire period, (d) Burn severity.

being respectively  $14.4\text{ }^{\circ}\text{C}$  and  $1330\text{ mm year}^{-1}$  ((SNIRH, 2020) and collected meteorological data from Pousada station ( $40.615083, -8.316333$ ) and Serra de Cima ( $40.609083, -8.321639$ ). The catchment is part of the Central Iberian zone and the geology consists of Pre-Ordovician metamorphic schist sediments and a greywackes complex (Boulet et al., 2015). Soils are predominantly a complex of Umbric and Dystric Leptosols and Humic Cambisols (Boulet et al., 2015; Pereira and FitzPatrick, 1995; Santos et al., 2016). On steep slopes the soils are shallow ( $0 - 30\text{ cm}$ ) Humic Cambisols with a silt-loam Ah-horizon overlying the schist bedrock (Pereira and FitzPatrick, 1995). The soil is classified as silt loam, with the silt fraction being  $50-60\%$  and the sand and clay fraction amounting to approximately  $20\%$  (Boulet et al., 2015). Field measurements revealed a high stone content in the catchment area, with a percentage in soil around  $40\%$  after the fire.

### 2.3. Catchment instrumentation

At the outlet of the catchment one hydrometric station was instrumented with an H-flume that had a maximum discharge capacity of  $0.861\text{ m}^3/\text{s}$ . The water level was measured at a timestep of  $5\text{ min}$  in duplicate by using a hobo® onset 13-Foot Water Level Data Logger and a Campbell Scientific® CS451 water level sensor connected to a CR1000 datalogger. The station also comprised one ISCO®3700 automatic sampler connected to the CR1000 with a maximum capacity of 24 bottles that collected runoff samples during rainfall events. The flume already existed from past experiments and was re-installed one week after the wildfire, which allowed for the creation of a complete record of all post-fire hydrological events. The runoff samples were filtered at the laboratory to quantify the Total suspended solids (TSS) by using a glass fiber filter and then dried in the oven to a constant weight at  $105\text{ }^{\circ}\text{C}$  (APHA, 1998).

Four automatic rainfall gauges (Pronamic Professional Rain Gauge with  $0.2\text{ mm}$  resolution) were installed, two at the top of the catchment,

one in Serra de Cima ( $40.609083, -8.321639$ ), and another in Pousada meteorological station ( $40.615083, -8.316333$ ) (Fig. 1.b). Four storage gauges (in-house design) were installed next to the automatic gauges to validate the automatic records.

### 2.4. Event selection and model parametrization

Each event was extracted from a continuous dataset obtained from Serra de Cima rainfall gauge with a timestep of  $1\text{ min}$ . The post-fire period considered was from September 2016 to July 2017, coinciding with the period when soil moisture data was available. From the dataset, 12 runoff events were extracted considering a minimum peak of  $0.007\text{ m}^3/\text{s}$ , with at least one hour without rainfall between events (Table 1). Events with more than two peaks and those lasting longer than  $24\text{ h}$  were excluded from this study, as the focus is on high-intensity events that can cause flash floods (Wu et al., 2021a). The events were then divided by random selection between calibration set (7 events) and validation set (5 events). The limited number of events selected is due to both the reduced availability of soil moisture data and the exceptionally dry year that 2017 was.

Quickflow for OpenLisem calibration was obtained by removing baseflow from streamflow using the automated separation technique proposed by Arnold et al. (1995). For sediments, only data collected by the autosampler up to December 2016 were used, as an exceptional event in early 2017 covered the flume with eroded material, reducing the reliability of the measurements. From the 6 events available in the shortened period, only 3 were detected and collected by the autosampler (d, h, i events – Table 1), and only in two of them the raising and descending limbs were identified (d, i events – Table 1). In order to fill the data gaps associated with sediment for the remaining events, a regression was performed between total suspended solids concentration and quickflow for OpenLISEM and flow for MOHID Land. Two different regressions were developed to consider ascending and descending limbs

**Table 1**

Runoff events and associated characteristics, including moisture characteristics and vegetation cover.

		Event code	API	p48	Ev. dur	vg_mdhg	θi_mdhg	θi_lwunb
CAL	23-Oct-16	a	44.31	16.60	0.00	0.07	7.53	18.00
	9-Nov-16	b	17.64	0.00	1.00	0.07	7.40	23.40
	21-Nov-16	c	57.60	55.60	0.00	0.19	7.63	19.30
	15-Dec-16	d	22.40	22.40	1.00	0.19	9.89	19.50
	7-Feb-17	e	63.10	16.80	1.00	0.21	16.70	25.40
	11-May-17	f	41.64	13.60	1.00	0.37	14.2	13.30
	28-Jun-17	g	3.27	3.20	1.00	0.42	5.25	8.30
VAL	20-Nov-16	h	10.19	23.00	1.00	0.19	10.57	17.90
	14-Dec-16	i	0.00	0.00	1.00	0.19	7.40	19.30
	3-Feb-17	j	21.89	27.20	0.00	0.21	15.37	28.10
	30-Mar-17	k	47.57	0.00	1.00	0.25	11.90	23.30
	30-Apr-17	l	0.00	0.00	1.00	0.25	7.60	17.90

separately. The regression for the ascending limb was exponential, with an R<sup>2</sup> equal to 0.91 and 0.93, while the regression for the descending limb was linear, with an R<sup>2</sup> of 0.72 and 0.40 for quickflow and total flow respectively.

API – antecedent precipitation index of the last 10 days prior to the event [-], p48 – antecedent precipitation in the previous 48 h before the event [mm], Ev.dur event duration coefficient being 0 events that last less than 1 h and 1 if it is more [-], vg – is the average vegetation cover obtained by fc values (mdhg – for moderate and high burn severity, vg equal to 0.4 reflects the average value for low burn severity, while 0.6 characterized unburned conditions), and θi is the initial soil moisture content (mdhg – values for moderate and high severity, lwunb – values for low severity and unburned conditions).

Given the high spatiotemporal resolution of OpenLISEM and MOHID Land models, detailed inputs are required to correctly run a simulation. The model input data are categorized into time-invariant and time-variant.

**2.4.1. Time-invariant data**

The designation “time-invariant” indicates input data remaining constant between events, being constant over time (Table 2). These data are further divided into constant and variable types within the

**Table 2**

Input data for OpenLISEM (left), for both models (center), and for MOHID Land (right).

Input data		OpenLisem		MOHID Land
Time-invariant	Spatially constant	PSI	SOILDEP	
		ROADWIDT		
	Spatially variable	RR		Water level
		D90		
Time variant	PER	AGGRSTAB	THETAS	ALPHA
		STONEFRC	CH	N_FIT
Calibrated	COH	COHADD	LAI	L_FIT
			THETAI	
		D50	KSAT	τs
		MANNING’S	RAINSplash	
		N		

PSI – water tension at the wetting front [cm], ROADWIDT – width of impermeable roads [m], RR – Random roughness [cm], D90 – D90 value of soil [μm], AGGRSTAB – Aggregate stability [-], SOILDEP – Soil depth of the layer [cm], Water level – water table altitude [%], STONEFRC – Stone fraction [-], COHADD – Additional cohesion by roots [kPa], THETAS – Saturated volumetric soil moisture content [-], CH – vegetation height [m], ALPHA – Van Genuchten inverse of air entry [m<sup>-1</sup>], N\_FIT – pore size distribution [-], L\_FIT – empirical core connectivity [m], PER – fraction of soil covered by vegetation [-], LAI – Leaf area index [-], THETAI – Initial volumetric soil moisture content [-], D50 – D50 value of soil [μm], COH – cohesion of bare soil [kPa], KSAT – Saturated hydraulic conductivity [mm hr<sup>-1</sup>], N – Manning’s n [-], τs – critical shear stress for erosion [Pa], RAINsplash – erosion coefficient from rain splash [mm hr<sup>-1</sup>].

catchment area, based on their spatial variations. The spatial variability in the input data was based on field observations and literature, such as in the case of stone fraction and volumetric soil moisture content, or variation in burn severity within the catchment, such as vegetation height (Table 3). For example, tree height was assumed to be 0 m in areas burned at moderate and high severity, while an average value of 10 m was given for low severity and unburned areas since most of the affected land use consisted of mixed forest (eucalyptus and acacia) and mature eucalyptus plantation stands between 3 and 7 years (Table 3). Root cohesion was assumed to be 0 kPa for high severity areas, while for the remaining severities root cohesion was considered equal to 10 kPa (Wu et al., 2021a) and unchanged by unburned conditions (Table 3).

**2.4.2. Time-variant data**

The term “time-variant” is used for inputs that change both in time and space, influenced by external factors such as vegetation recovery or weather conditions (Table 2). Vegetation indexes such as the leaf area index (LAI) and the fraction of soil covered by vegetation (PER) were obtained from Sentinel 2 images (Table 3). The LAI was extracted from Baret and Guyot (1991) equation:

$$VI = VI_{\infty} + (VI_g - VI_{\infty}) * \exp(-K_{VI} * LAI) \tag{1}$$

Where VI is the vegetation index from the satellite, VI<sub>g</sub> corresponds to the bare soil value, VI<sub>∞</sub> to the highest value detected in the area, and K<sub>VI</sub> is a coefficient that controls the slope of the relationship, fixed to 0.5 (value for eucalyptus globulus Breda (2003)). The PER parameter was derived from the equation introduced by Qi et al. (2000) which, based always on the VI, provides the fractional green vegetation cover (fc).

$$fc = \frac{VI - VI_g}{VI_{\infty} - VI_g} \tag{2}$$

Different vegetation indices (NDVI – Normalized Difference Vegetation Index, TSAVI – Transformed Soil Adjusted Vegetation Index (Baret et al., 1989), and MSAVI – Modified Soil Adjusted Vegetation Index (Qi et al., 1994)) were compared to see which one best represented the study area. Ground cover data were collected from 9 different 0.25 m<sup>2</sup> plots within the catchment, with 2 months intervals since the fire. Such data collection consisted of identifying the main cover features, such as stones, ash, bare soil, litter, and vegetation, through the analysis of field photographs. A comparison was made between the ground vegetation cover monitored in the plots and the fc values obtained from the remote sensed indices. The TSAVI was found to be the most suitable to represent vegetation in this location.

The initial soil moisture content (THETAI) was collected continuously in the field covering a period from 2012 to July 2017. Pre-fire data were collected in one location, while instruments for the collection in the post-fire period were installed in four different catchment points, covering areas defined as unburned, moderate and high burn severity.

**Table 3**  
Model input values and spatial variability.

Map type	Model input	Value	Unit	Spatial resolution	Source	
Time-invariant	PSI	16.68	cm	Catchment	Rawls et al. (1983)	
	ROADWIDT	3	m	Catchment	Field data	
	D90	177	$\mu\text{m}$	Catchment	Field data	
	SOILDEP	30	cm	Catchment	Field data	
	AGGRSTAB	30	–	Catchment	Wu et al., (2021a)	
	Water Level	30	%	Catchment	Model warm-up	
	N_FIT	1.47	–	Catchment	Field data	
	L_FIT	0.33	m	Catchment	Field data	
	THETAS	0.07–0.17	–	Land cover	Field data	
	RR	1–1.19	cm	Land cover	Wu et al., (2021a)	
	STONEFRFC	0.13–0.65	–	Land cover/Soil type	Field data	
	COHADD	0–10	kPa	Burn severity	Wu et al., (2021a)	
	CH	0–10	m	Burn severity	Land use	
	ALPHA	0.69–3.43	$\text{m}^{-1}$	Burn severity	Field data	
	Time-variant	LAI	0–4.5*	–	Pixel	Sentinel 2
		PER	0–0.9*	–	Pixel	Sentinel 2
THETA1		0.05 – 0.28*	–	Burn severity	Field data	

\*values are different for each event.

### 2.5. Calibration approach and model performance

Calibration of the hydrologic response was based on model's performance in simulating quickflow for OpenLISEM and flow for MOHID Land by adjusting the hydraulic conductivity (Ksat) and resistance to flow (Manning's n) parameters. The hydraulic conductivity (Ksat), which controls the amount of rainfall that can infiltrate, is generally modified to account for reduced infiltration rates in post-fire conditions (Ebel and Moody, 2020; Robichaud et al., 2007; Srivastava et al., 2018; Thomas et al., 2021; Vieira et al., 2022; Wu et al., 2021b). Manning's n, which represents the terrain roughness applied to the flow, is adjusted to reflect increased peak runoff and faster-rising limb of such peaks (Rulli and Rosso, 2007; Thomas et al., 2021; Vieira et al., 2022; Wu et al., 2021b).

The autocalibration for the hydrological response used the Prince (1977) Pseudo-random Search Optimization Algorithm and was used to narrow the Ksat and Mannings n values within an acceptable range. Using the OpenLISEM model, the process consisted of 1000 simulations with wide ranges for both Ksat (0–70  $\text{mm h}^{-1}$ ) and Manning's n (0–1). Considering as acceptable the runs with statistical parameters  $\text{KGE} > -0.41$  and  $\text{wR}^2 > 0.25$  (Eq. (3) and (4)), the autocalibration provided a set of values for each event, considered as the local conditions of the catchment (Fig. 2).

To obtain consistent calibrated parameters applicable to the validation set across all events, the spatiotemporal variability of Ksat and Manning's n was considered (Fig. 2). The temporal variability, influenced by the initial moisture conditions and vegetation cover of each specific rainfall event (Table 1), was addressed through the use of regression analysis. The spatial variability of the two parameters was based on burn severity, assuming a decrease in value with increasing severity (Cerdà, 1998; Ebel and Moody, 2020; Robichaud, 2000). In burned areas with moderate and high severities within the catchment, hydrological parameters were assumed equal, since field measurements at plot scale observed a negligible difference in runoff between the two severities. The spatial variability was integrated into the parametrization through a constant that increases with increasing severity. Therefore, for the validation set, the hydrological parameters were derived from a regression analysis considering the API – antecedent precipitation index of the last 10 days prior to the event, p48 – antecedent precipitation in the previous 48 h before the event, ev.dur – event duration coefficient, vg – average vegetation cover, and  $\theta_i$  – initial soil moisture content of each event (Table 1) as the values of the independent variables.

A sensitivity analysis was performed to assess the impacts of event moisture and vegetation conditions on Ksat and Manning's n values. A first-order variance-based sensitivity analysis (Sobol' method (Sobol',

1990)) was performed using the sensitivity package in R (Iooss et al., 2021) based on 10,000 runs. Due to computational limitations the uncertainty analysis could only be performed for OpenLISEM and not for MOHID Land, which is reflected in the absence of such results for both models in the current work.

OpenLISEM and MOHID Land parameterization of sediment yield lacked direct correlation due to different equations utilized in the models. Therefore, in this case an initial autocalibration does not benefit the calibration process. The calibration was based on COH and D50 parameters for OpenLISEM (Wu et al., 2021b), and critical shear stress and erosion coefficient to splash erosion for MOHID Land. These parameters are sensitive to burn severity (Mataix-Solera et al., 2011; Moody et al., 2005), leading to spatial variability considerations.

Model performance was assessed separately for each event and through an overall assessment with respect to peak stream flow, time of the peak, discharge and sediment yield at the catchment outlet. To evaluate model performance for an event, the coefficient of determination  $\text{R}^2$ , as well as its weighted version  $\text{wR}^2$  (Krause et al., 2005), were computed using (Eq. (3)).

$$\begin{cases} \text{wR}^2 = |b|\text{R}^2_{\text{forb}} \leq 1 \\ \text{wR}^2 = |b|^{-1}\text{R}^2_{\text{forb}} > 1 \end{cases} \quad (3)$$

Where  $\text{R}^2$  is the coefficient of determination and b is the gradient on which  $\text{R}^2$  is based. Together with  $\text{wR}^2$ , gradient b was also discussed to quantify the model under- or over-predictions.  $\text{R}^2$  and  $\text{wR}^2$  values close to 1 indicate a good model prediction (Moriassi et al., 2015).

The Kling-Gupta efficiency (KGE) (Gupta et al., 2009) (Eq. (4)) was also used since Nash-Sutcliffe efficiency (NSE) is not recommended for evaluating model performance for individual events (Krause et al., 2005; Moriassi et al., 2015).

$$\text{KGE} = 1 - \sqrt{(r-1)^2 + (\alpha-1)^2 + (\beta-1)^2} \quad (4)$$

Where  $\alpha$  is a measure of relative variability among the simulated and observed values, calculated as the ratio of the standard deviations of the simulated and observed values,  $\beta$  is the normalized bias by the observed standard deviation, and r is the Pearson product-moment correlation coefficient. Unlike the majority of model performance coefficients, such as  $\text{R}^2$  and NSE, KGE negative values do not indicate unsatisfactory model performance. Reasonable values of KGE range between  $-0.41$  and 1 (Knoben et al., 2019).

For the overall assessment, the coefficient of determination  $\text{R}^2$ , its weighted version  $\text{wR}^2$ , and the Nash-Sutcliffe efficiency (NSE; Moriassi et al., 2015) were used. Model performance for the overall assessment was based on the limits recommended by Moriassi et al. (2015), considered satisfactory for values of  $\text{R}^2 > 0.6$  and  $\text{NSE} > 0.5$  for the

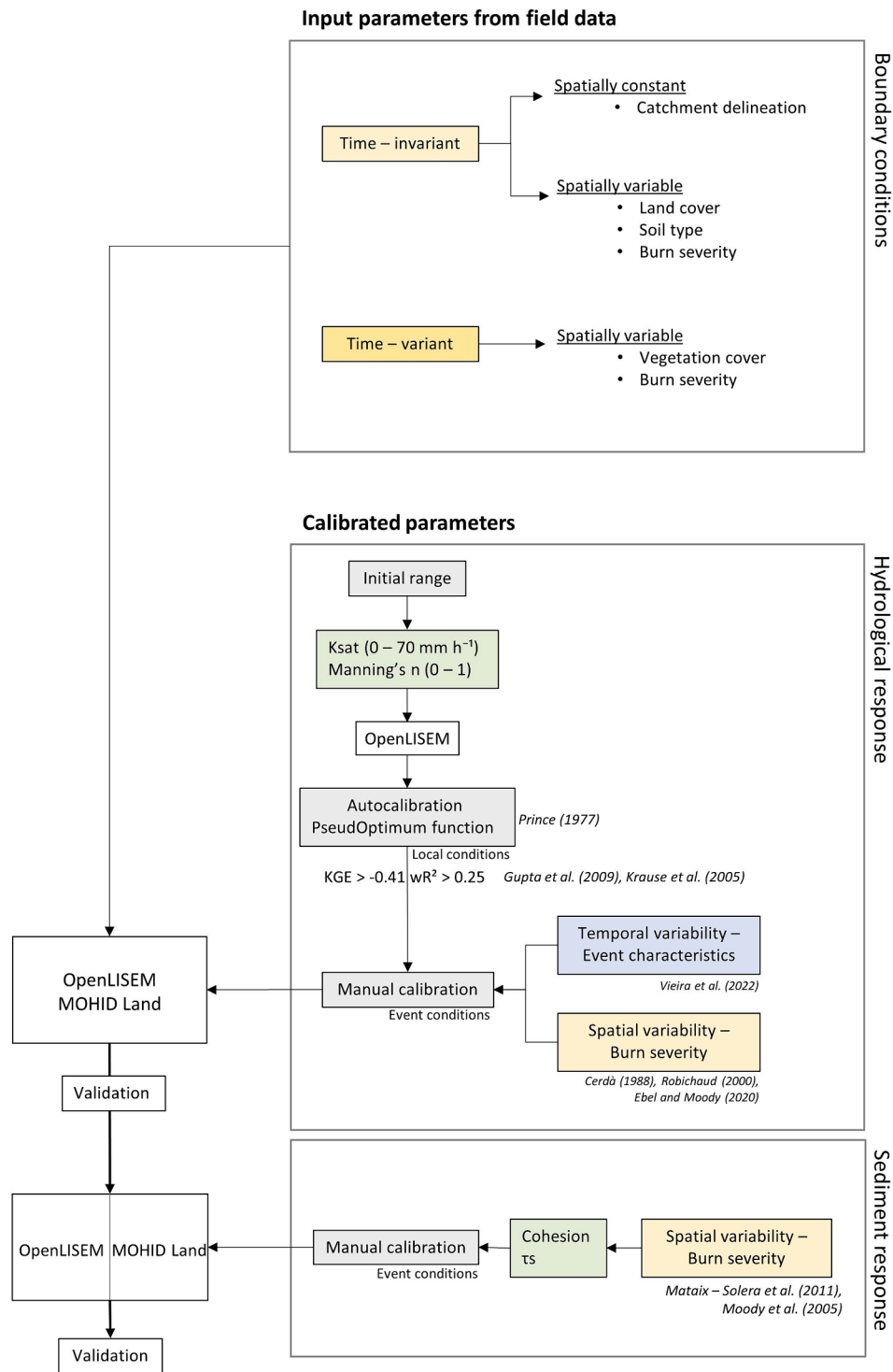


Fig. 2. Modelling approach scheme.

hydrological response and  $R^2 > 0.4$  and  $NSE > 0.45$  for the sediment transport.

### 3. Results

#### 3.1. Calibration and validation of the hydrological response at catchment scale

The methodology proposed in this study aimed to incorporate the spatiotemporal variability of Ksat and Manning’s n into the calibrated

values. From the regression analysis, a set of unstandardized coefficients was derived and used to obtain the specific Ksat and Manning’s n values for each event (Table 4).

Calibrated Ksat values for the moderate and high severity burn areas were between 3.43 and 7.96 mm h<sup>-1</sup>, for the low severity area; in a range between 5.26 and 10.25 mm h<sup>-1</sup>, and for the unburned area between 9.10 and 14.09 mm h<sup>-1</sup> (Table 5). The average reduction ratio in Ksat for high/moderate severity with respect to unburned conditions ( $Ksat_{burned}/Ksat_{unburned}$  (Ebel, 2019)) was 0.44, which is greater than what was found for Manning’s n (0.71). Moreover, differences between

**Table 4**  
Ksat and Manning’s unstandardized coefficients for different burn severities.

		Constant	API	p48	Ev dur	vg	θi
Ksat	High – Moderate	2.17	−0.01	0.13	3.24	−3.88	−0.01
	Low	5					
	Unburned	10					
Manning’s n	High – Moderate	0.35	−0.001	−0.003	0.03	0.03	−0.01
	Low – Unburned	0.5					

**Table 5**  
Ksat and Manning’s n values for each event.

Event		Ksat (mm h <sup>−1</sup> )			Manning’s n (−)	
		High – Moderate	Low	Unburned	High – Moderate	Low. Unburned
CAL	a	3.43	4.95	9.10	0.17	0.24
	b	4.82	6.61	10.45	0.29	0.31
	c	7.96	10.25	14.09	0.04	0.09
	d	7.24	9.56	13.39	0.20	0.27
	e	5.80	8.20	12.04	0.10	0.18
	f	5.07	8.18	12.02	0.16	0.30
	g	4.11	7.37	11.21	0.33	0.46
VAL	h	7.48	9.82	13.66	0.20	0.30
	i	4.60	6.89	10.73	0.32	0.37
	j	4.52	6.88	10.72	0.10	0.14
	k	3.67	6.20	10.04	0.22	0.27
	l	4.36	6.90	10.74	0.32	0.38

unburned and low severity Manning’s n were minor, leading to the incorporation of the variables into a single category. Manning’s n values ranged from 0.04 to 0.33 for high and moderate burn severity, and from 0.09 to 0.46 for low severity and unburned conditions (Table 5).

The sensitivity analysis revealed a high sensitivity of Ksat for the precipitation preceding the event (p48 [mm]) and the duration of the event itself (Ev dur [-]) (Fig. 3.a). When analyzing Ksat’s variability between events (Fig. 4) we observed how the Ksat values increased during autumn and winter and decreased afterwards. Manning’s n appeared to be sensitive to the combined effect of pre-event precipitation and soil moisture conditions (Fig. 3.b). A seasonal trend of Manning’s n can also be observed in Fig. 4, with increasing values as precipitation decreases.

OpenLISEM predicted the quickflow of the individual events of the calibration set with a satisfactory to good model performance in terms of R<sup>2</sup> (Table 6) for events a, c (Fig. 5.a), d and g. OpenLISEM fails to simulate the two peaks of event b (Supplementary material Figure S1) and the first peak of event f (Fig. 5.b), not achieving a satisfactory performance (R<sup>2</sup> ≤ 0.6). Underprediction in terms of R<sup>2</sup> was also observed for event e as OpenLISEM was unable to predict the correct magnitude of the second peak (Supplementary material Figure S1). The weighted coefficient wR<sup>2</sup> reflected the underprediction of events b and e, as shown by the gradient values b around 0.4 and the corresponding

wR<sup>2</sup> value (Table 6). The KGE values revealed good model performance (Gupta et al., 2009; Knoben et al., 2019), with the lowest predicted value for event f (KGE = -0.19), which also presented an overestimation of the simulated quickflow, as indicated by the gradient value b = 1.22. The overprediction indicated by b values greater than 1 seems to be attributed to the milder slope gradients of the hydrographs of the simulated events.

When considering the overall performance of the calibration set, OpenLISEM performance for the total quickflow was satisfactory, but, as mentioned above, appeared to be biased by the steepness of the hydrographs of the individual events, thus resulting in overprediction of the total volume. OpenLISEM performance in simulating the peak discharge was satisfactory in terms of R<sup>2</sup> and NSE, while good model performance was obtained in simulating the time of the peak, confirmed by the gradient of the slope close to 1 (b = 1.14).

Validation results of individual events were not as good as calibration results. OpenLISEM performance in terms of R<sup>2</sup> was good, except for event i where the model failed to simulate the first smaller peak of the hydrograph (Supplementary material Figure S2). Even if performing well in terms of R<sup>2</sup>, OpenLISEM overestimated peak discharge for events h, k and l (Supplementary material Figure S2). In particular, the model was found to be unable to predict event h, simulating a peak discharge of 1.19 m<sup>3</sup>/s when observations show a peak of 0.33 m<sup>3</sup>/s.

OpenLISEM performance in predicting the total and the peak discharge was not satisfactory in terms of wR<sup>2</sup> and NSE due to the overestimation of the peak discharge in the majority of the events, as indicated by b values. Nevertheless, the time of the peak was correctly simulated with a slope gradient b = 1.06 and an NSE = 0.98.

The performance of MOHID Land for individual events of the calibration set was satisfactory for events b, c (Fig. 5.c), e and g in terms of R<sup>2</sup> (Table 7). Based on R<sup>2</sup>, unsatisfactory performance of event a originated from its overestimation, while the milder slope grades of the hydrograph of event d and f seemed to explain the reduced values (Supplementary material Figure S3). wR<sup>2</sup> values reflected a good prediction of each event’s hydrograph, except for event b, where a large value of b (1.72) suggested model overestimation (Table 7). As for OpenLISEM, also MOHID Land failed to predict the presence of more than one peak in the hydrograph. MOHID Land was unable to reproduce the presence of a reduced first peak both in events e and f (Fig. 5.d), which, however, did not appear to affect model performance (Table 7). The statistical analysis performed with KGE showed a satisfactory model performance (Gupta et al., 2009; Knoben et al., 2019), with values larger

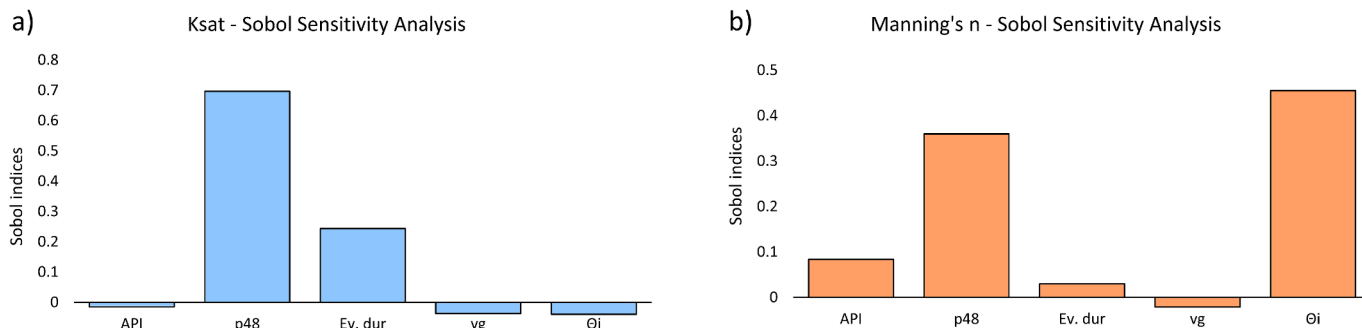


**Fig. 3.** Sensitivity analysis for Ksat and Manning’s n coefficient.

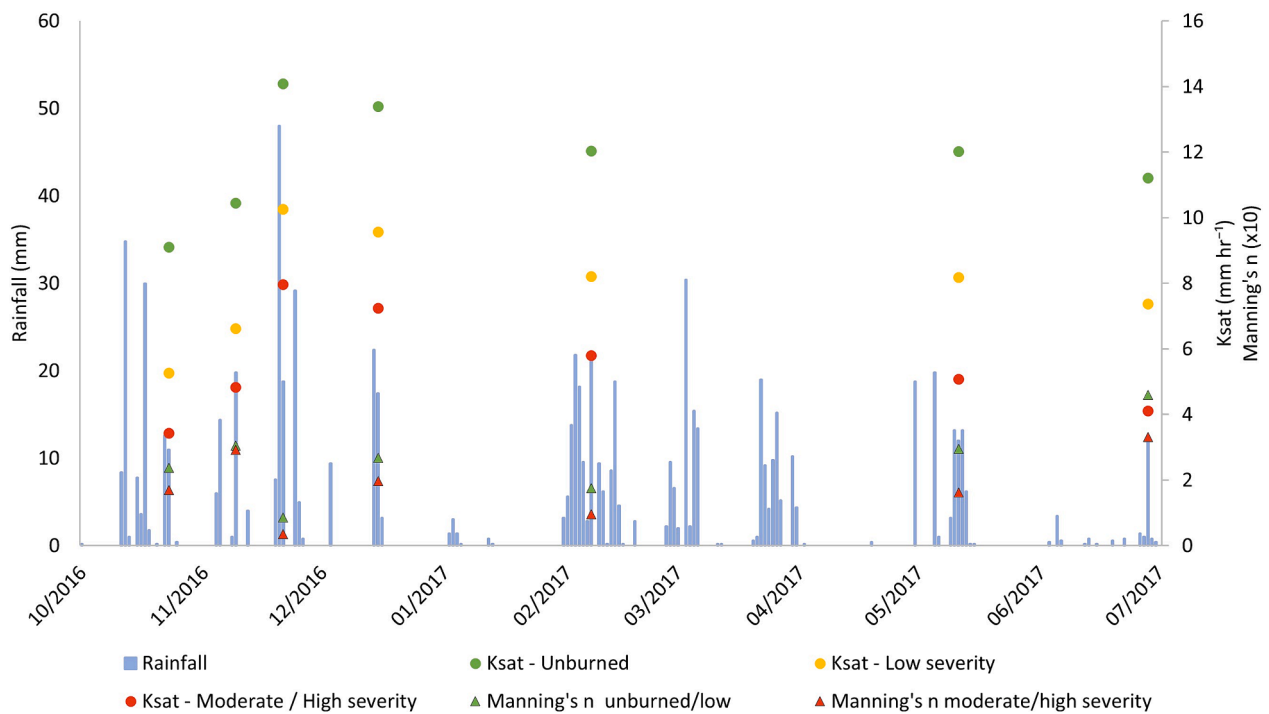


Fig. 4. Calibrated Ksat and Manning's n variability during the simulated period.

Table 6  
OpenLISEM model efficiency for simulating quickflow.

		OpenLISEM															
Event	Individual events					Total discharge				Peak discharge				Time peak			
		R <sup>2</sup>	b	wR <sup>2</sup>	KGE	R <sup>2</sup>	b	wR <sup>2</sup>	NSE	R <sup>2</sup>	b	wR <sup>2</sup>	NSE	R <sup>2</sup>	b	wR <sup>2</sup>	NSE
CAL	a	0.72	1.12	0.65	0.63	0.66	1.24	0.53	0.10	0.67	0.63	0.43	0.54	0.97	1.14	0.85	0.95
	b	0.34	0.43	0.15	0.33												
	c	0.81	0.49	0.40	0.26												
	d	0.86	1.15	0.75	0.23												
	e	0.41	0.40	0.16	0.48												
	f	0.57	1.22	0.47	-0.19												
	g	0.73	0.66	0.48	0.70												
VAL	h	0.87	4.00	0.21	-4.00	0.97	4.95	0.20	<0	0.98	3.88	0.25	<0	0.99	1.06	0.94	0.98
	i	0.14	0.55	0.08	-0.30												
	j	0.88	0.75	0.54	0.80												
	k	0.82	3.75	0.22	-4.68												
	l	0.65	2.27	0.29	-1.51												

than 0 indicating good calibration.

For the calibration set, MOHID Land showed satisfactory performance in the simulation of the overall total discharge and peak flow rate and a very good ability to simulate the time of the peak (Table 7). The milder slope gradient of events d and f and the overestimation of event b resulted in an overall overprediction of the total discharge (b = 1.38).

The performance of the MOHID Land for events h and l in the validation group was good in terms of R<sup>2</sup>, but not in terms of b and wR<sup>2</sup>, which revealed a substantial overestimation (Table 7). MOHID Land predicted peak values that were three times higher than those observed (event h: 0.89 vs. 0.38 m<sup>3</sup>/s; event l 0.086 vs. 0.028 m<sup>3</sup>/s). Although model performance based on R<sup>2</sup> for events j and k was unsatisfactory, the KGE values show good results, confirmed also by the graphical analysis of the two events (Supplementary material Figure S4).

The performance of MOHID Land for single event validation (Table 7) was better than that of OpenLISEM. Although performance in terms of R<sup>2</sup> is lower, wR<sup>2</sup> and KGE values showed a better hydrograph prediction (Table 7, Supplementary material Figure S4).

The overall MOHID Land performance for the validation was

satisfactory, showing good agreement between observed and simulated peak discharge and time of the peaks. The high b values for total discharge and peak flow reflected the overestimation of the mentioned events affecting the wR<sup>2</sup> final value. The performance of the total discharge was less satisfactory, characterized by an unsatisfactory NSE value, biased by the two overestimated events in the validation group.

### 3.2. Calibration and validation of the sediment transport at catchment scale

Because of the limited number of events for sediment calibration, events h and i of the hydrological response validation set were used as events for sediment calibration. To obtain a reliable sediment yield prediction, Ksat for event h was adjusted to correctly represent the hydrological response during this event.

OpenLISEM was not sensitive to changes in D50, whose calibrated value for the entire watershed and all events resulted equal to 80 μm. Cohesion (COH) was the most sensitive parameter when calibrating sediment yield, being slightly sensitive to burn severities, decreasing

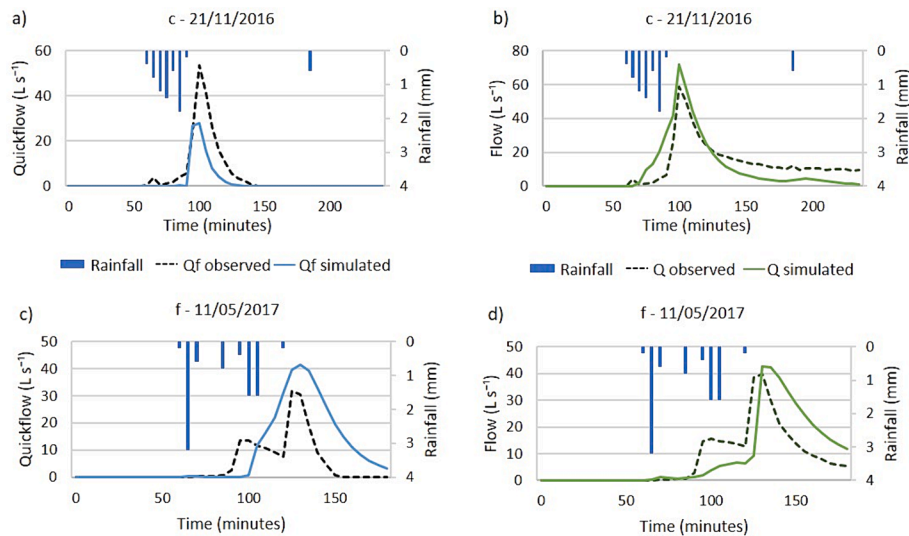


Fig. 5. A, b– Graphical representation of simulated and observed quickflow for two events of the calibration set using OpenLISEM. c, d – Graphical representation of simulated and observed flow for two events of the calibration set using MOHID Land.

Table 7  
MOHID Land performance for simulating flow.

		MOHID Land															
	Event	Hydrograph				Total discharge				Peak discharge				Time peak			
		R <sup>2</sup>	b	wR <sup>2</sup>	KGE	R <sup>2</sup>	b	wR <sup>2</sup>	NSE	R <sup>2</sup>	b	wR <sup>2</sup>	NSE	R <sup>2</sup>	b	wR <sup>2</sup>	NSE
CAL	a	0.36	1.05	0.33	0.12	0.91	1.38	0.66	0.43	0.74	0.57	0.42	0.69	0.98	0.94	0.93	0.99
	b	0.76	1.72	0.44	-0.10												
	c	0.79	1.13	0.70	0.69												
	d	0.35	0.86	0.33	0.19												
	e	0.71	1.11	0.64	0.60												
	f	0.54	0.89	0.48	0.63												
VAL	g	0.88	1.20	0.73	0.48												
	h	0.86	2.91	0.30	-1.60	0.99	2.50	0.40	<0	0.97	2.47	0.39	0.56	0.99	1.01	0.96	0.98
	i	0.34	1.09	0.31	-0.47												
	j	0.31	0.61	0.19	0.51												
	k	0.15	0.53	0.08	0.09												
	l	0.95	3.82	0.25	-2.73												

with increasing severity. The calibrated value of COH for unburned and low severity conditions was 700 kPa, and for moderate and high burn severity it was found to be 600 kPa.

Nevertheless, a COH value of 600 kPa led to a strong underestimation of the sediment peak of event h (observed = 29.33 kg s<sup>-1</sup>, simulated = 9.65 kg s<sup>-1</sup>), which was instead correctly simulated using COH values of 10 kPa (event h\*) for moderate and high severity (observed = 29.33 kg s<sup>-1</sup>, simulated = 33.74 kg s<sup>-1</sup>).

OpenLISEM performance for individual events in the calibration set was not satisfactory when considering the values obtained from the KGE analysis for events i and d (Table 8). Peak sediment yield was simulated correctly for both event d (Fig. 6.a) and i, but the milder slopes obtained for the respective hydrographs biased the performance of OpenLISEM (Supplementary material Figure S5). The overall performance of OpenLISEM was satisfactory in terms of R<sup>2</sup>, wR<sup>2</sup> and NSE for the sediment volume and time of the peak. Peak sediment yield prediction was negatively affected by the underestimation of event h, resulting in a wR<sup>2</sup> of 0.31 and an unsatisfactory NSE value. A reduction in the overall performance for the sediment volume in terms of wR<sup>2</sup> and NSE is observed when considering event h\*.

Considering the validation set, OpenLISEM performance for individual events resulted in low R<sup>2</sup> values but satisfactory KGEs, in particular for event a (Fig. 6.b). B values for events b and c revealed an underestimation of the peak. OpenLISEM inability to reproduce the two

peaks for event b is reflected in the performance of the model to simulate the sediment yield for the event (Supplementary material Figure S6).

OpenLISEM overall performance for the validation was satisfactory in terms of R<sup>2</sup>, however the underestimation of events b and c was reflected in b and wR<sup>2</sup> values for the total sediment yield and the peak value (Table 8). A very good performance was obtained for the time of the peak, confirmed by all the statistical parameters (Table 8).

Critical shear stress, the input used in MOHID Land to simulate sediment yield, was not sensitive to spatial variability based on burn severity. The calibrated critical shear stress was 1.2 N m<sup>-2</sup>, while the erosion coefficient for rain splash was equal to 1.0E-10 g J<sup>-1</sup>. As observed in OpenLISEM calibration, event h was underpredicted using the same coefficient as the other events, but was correctly simulated using a rain splash value of 1.0E-5 g J<sup>-1</sup> (event h\*\*).

MOHID Land performance for each event of the calibration group was not satisfactory when analyzing R<sup>2</sup> and wR<sup>2</sup> values for events h and i (Table 8), while it revealed a satisfactory performance for event d (Table 8, Fig. 6.c). The overall performance was not satisfactory, largely biased by event h, which was underestimated, with a simulated peak of 845 g s<sup>-1</sup> compared to the 53139 g s<sup>-1</sup> of the observed event. Always biased by the largest event, the overall performance was good when considering event h\*\*.

MOHID Land performance for the individual events for the validation set was satisfactory only for event c in terms of R<sup>2</sup>, wR<sup>2</sup> and KGE.

**Table 8**  
OpenLISEM and MOHID Land model performance for simulating sediment transport.

OpenLISEM															
Event	Individual events			KGE	Total yield			Peak			Time peak				
	R <sup>2</sup>	b	wR <sup>2</sup>		R <sup>2</sup>	b	wR <sup>2</sup>	R <sup>2</sup>	b	wR <sup>2</sup>	R <sup>2</sup>	b	wR <sup>2</sup>	NSE	
CAL	h	0.28	0.24	0.10	0.28	0.84	0.84	0.95	1.00	0.32	0.32	0.99	1.08	0.91	1.00
	h*	0.80	0.64	0.50	-1.00	2.85*	0.35*	<0*	1.00*	1.14*	0.88*	0.99*	1.08*	0.91*	1.00*
	i	0.10	0.71	0.10	-3.23										
VAL	d	0.70	1.81	0.39	-1.44										
	a	0.19	0.55	0.11	0.31	0.37	0.37	0.03	1.00	0.44	0.44	0.99	1.19	0.83	0.99
	b	0.25	0.25	0.06	0.09										
c	0.38	0.29	0.11	0.14											
<b>MOHID Land</b>															
CAL	h	0.30	0.00	0.00	-0.42	0.05	0.05	<0	0.98	0.01	0.01	0.98	1.06	0.92	0.93
	h**	0.96	0.95	1.02	0.77	1.95**	0.51**	0.87**	1.00**	1.00**	1.00**	0.98**	1.06**	0.92**	0.93**
	i	0.08	0.34	0.01	-0.25										
VAL	d	0.64	0.69	0.23	0.76										
	a	0.23	16.00	0.01	-39.52	1.77	0.49	<0	0.30	0.10	0.03	1.00	0.98	0.98	0.99
	b	0.36	1.61	0.23	-1.09										
c	0.75	1.03	0.73	0.50											

\*Event h parametrized with COH = 10 kPa. \*\* Event h parametrized with 1.0E-5 g J<sup>-1</sup>.

MOHID Land failed to simulate events a and b, for which the over-estimation was biased by the corresponding simulated hydrographs. The overall performance of MOHID Land was not satisfactory, in this case affected by the large overprediction of event a (b = 16 and KGE = -39.52) (Fig. 6.d).

## 4. Discussion

### 4.1. Calibration procedure

#### 4.1.1. Hydrological response

The range of post-fire Ksat values (3.43–10.25 mm hr<sup>-1</sup>, Table 5) obtained from the calibration were in the same order of magnitude as the values calibrated for the first post-fire year in other studies (0.039–3.36 mm hr<sup>-1</sup> Canfield et al. (2005), 10.40–18.32 mm hr<sup>-1</sup> Chen et al. (2013), 1.00–10.00 mm hr<sup>-1</sup> Rengers et al. (2016)). In this study, the ratio of Ksat between areas of moderate and high burn severities compared with the value in unburned areas was 0.44, which is in agreement with the reductions estimated by Ebel and Moody (2020) (0.37) and Ebel (2019) (0.30). Conversely, Wu et al., (2021b) modeled a slight increase in Ksat in post-fire conditions, explained by the authors as the impacts of macropore formation due to root burning. The Ksat values obtained for the unburned area reflected typical values of deep-plowed soils, common in eucalyptus plantations (Madeira, 1989). Increased compaction and decreased aggregate stability in eucalyptus plantations reduce total porosity, affecting saturated hydraulic conductivity (Madeira, 1989).

The range of post-fire Manning's n values (0.04–0.33, Table 5) obtained from the calibration were in agreement with values from other modeling studies performed in Portugal (0.24–0.6 Vieira et al. (2022), 0.07 Wu et al., (2021a)). Canfield et al. (2005) estimated Manning's n values between 0.014 and 0.43, while other post-fire modeling studies suggested values similar to those used for bare soil (0.015–0.055) (Chen et al., 2013; Moody and Kinner, 2006; Rulli and Rosso, 2007, 2005). Vieira et al. (2022), explained the relatively high Manning's n values by the typical soil interventions in the area, such as ploughing and terracing (Martins et al., 2013). In addition, the high amount of stones in the soil surface could contribute to surface heterogeneity and increase the surface roughness value (Kutiel et al., 1995).

The increase in resolution during the post-fire window of disturbance was expected to benefit the estimation of the magnitude and the timing of the hydrological response, especially following heavy rainstorms that could lead to destructive off-site effects. However, the application of a generalized calibration for event-scale modeling appeared to be a drawback linked with using simulation at such temporal resolution for wildfire impact predictions (Baartman et al., 2012; Rengers et al., 2016; Vieira et al., 2022; Wu et al., 2021a). In this study, a methodology was conceived to obtain a generalized calibration for the hydrological response based on the event boundary conditions. This approach would simplify the setting of validation parameters, not relying on temporally constant calibrated factors, which values are notably influenced by moisture conditions. Instead, the parametrization was based on specific event characteristics.

High spatiotemporal variability of Ksat and Manning's n was obtained as a function of soil properties and extrinsic factors such as land cover and precipitation. Baartman et al. (2012) observed that large infiltration surface area caused Ksat to increase with increasing rainfall intensity, while Vieira et al. (2022) found great sensitivity of the hydrological response to event-specific conditions, as rainfall characteristics and time since fire interfered with hydrological parameters such as Ksat, Manning's n and θ<sub>s</sub>. The large influence of the (antecedent) rainfall characteristics of each event on Ksat (Fig. 3) emphasized the relationship between the overland flow and the antecedent wetness state for each event. The seasonal behavior of Ksat and Manning's n (Fig. 4) could represent the dominant processes inducing runoff generation. Previous studies performed in the area evidenced a strong variation in the runoff

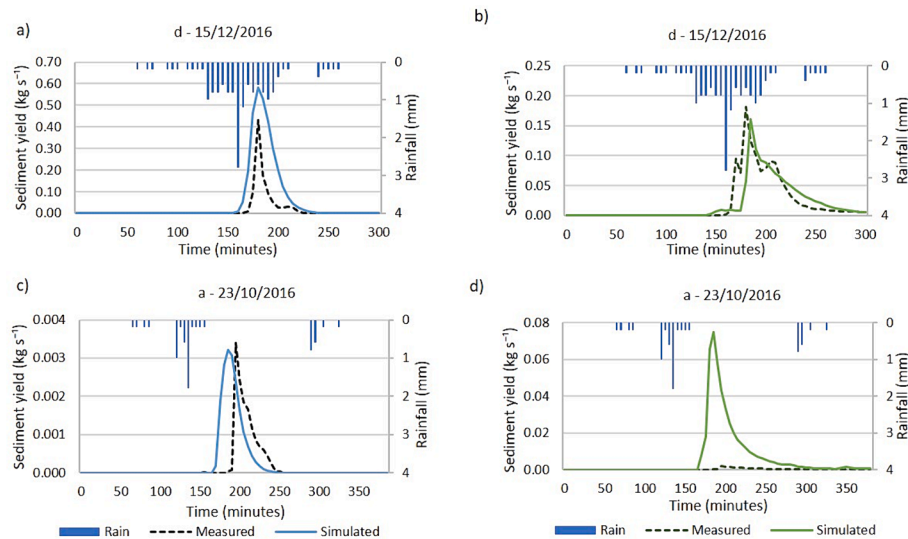


**Fig. 6.** A, b – Graphical representation of simulated and observed sediment yield for one event in the calibrated (a) and validated (b) set using OpenLISEM. c, d – Graphical representation of simulated and observed sediment yield for one event in the calibrated (c) and validated (d) set using MOHID Land.

generation processes between dry and wet seasons (Boulet et al., 2015; Ferreira et al., 2000; Santos et al., 2016). Following a wildfire, soil water repellency can intensify Hortonian overland flow during the dry period, resulting in a more significant contrast with the wet period, when repellency is reduced and runoff is predominantly generated by saturation overland flow (Doerr and Thomas, 2000; Ferreira et al., 2000; Keizer et al., 2008; Leighton-Boyce et al., 2005; Vieira et al., 2018a). The variability of soil water repellency, along with variability in natural runoff generation, emphasized the significance of considering the temporal variation of Ksat and Manning's n calibrated values with the wetness state of each event.

Calibration of post-fire runoff events by Canfield et al. (2005) revealed an increasing hillslope roughness and saturated hydraulic conductivity over time associated with vegetation growth after fire. The events analyzed by Canfield et al. (2005) covered a longer period than those studied here, explaining why this behavior was not observed. Other studies summarized by Ebel and Martin (2017) measured recovery of the saturated hydraulic conductivity over time, reporting a noticeable increase after one year from the fire occurrence. From studies modeling longer periods (Canfield et al., 2005; Vieira et al., 2022), the importance of relating Ksat values with time since fire became clear. In addition, the implementation of emergency measures after the fire, which aim to mitigate impacts and improve vegetation recovery (Girona-García et al., 2021), may require adaptation of the model to these circumstances (Basso et al., 2022b; De Girolamo et al., 2022; Vieira et al., 2014). In the Serra de Cima basin, no post-fire measures were carried out in the first year after the fire. In this work, the relationship between Ksat and Manning's n coefficient with the variable of time since fire, represented as vegetation cover, was limited because of the short period analyzed. As mentioned, the brevity of the selected period was due to the discontinuation of the soil moisture data collection. Remote sensing data could provide additional soil moisture data after being previously calibrated. Future work in the region should extend these measurements beyond the first year after the fire, in order to assess the sensitivity of Ksat and Manning's n not only to the hydrological characteristics but also to the recovery process.

#### 4.1.2. Erosive response

Cohesion values calibrated or measured in previous OpenLISEM applications were below 100 kPa for both forests (Baartman et al., 2012), eucalyptus plantations (Ebling et al., 2021), and burned areas (Wu et al., 2021a). The high cohesion values in the area (600 – 700 kPa)

could reflect the stony character of the soil in the watershed (Boulet et al., 2021, 2015; Shakesby et al., 1996). The extent of post-fire erosion in thin and stony soils is limited compared with other environments (Coelho et al., 1995; Shakesby, 2011). Erosion rates measured in the Agueda basin, which includes Serra de Cima catchment, were over one order of magnitude lower than those measured in the first year after fire in other burned areas (Coelho et al., 1995). In stony soils, only a limited amount of material remains available for transport after surface ash and charred debris are removed by the first heavy rainstorms (Shakesby and Doerr, 2006). The lower cohesion value (10 kPa) required to correctly simulate event h could be explained by the transport of the ash layer during this event, characterized by greater runoff than the other events. The high cohesion values (600 kPa) of previous events (events a and b), could represent less sediment movement due to the smaller magnitude of these events. It also appeared that low magnitude events failed to connect the entire catchment area, causing the movement of sediment and ash probably from the vicinity of the outlet. Likewise, ash and sediments might have been retained in the system and been flushed away during the large event (Murphy et al., 2019). These phenomena might explain why OpenLISEM required very high COH values to mimic the small/local sediment movement and the stony character of the soil.

MOHID Land parametrization of the critical shear stress value was within the range proposed by Moody et al. (2005), who measured the variability of the critical shear stress with fire temperature in a laboratory experiment, finding that the value fluctuates between 0.5 – 2 N m<sup>-2</sup> for temperatures between 175 and 275 C. Considering the rain splash coefficient for soil erosion, it seemed that the calibrated values, in the order of E-10, corresponded to poorly erodible soils reflecting the high stone content. The larger rain splash coefficient that best simulated event h allowed the prediction of higher sediment transport, ratifying what was discussed in the case of OpenLISEM. In this study, the values obtained during the calibration of sediment transport variables emphasized the importance of considering the magnitude of the rainfall event when parameterizing the model. The large discrepancy in values used for event h compared to the other events reflected the influence of rainfall intensity on the overall catchment connectivity. Differences in the calibration values between events likely indicated the adaptation of the model to replicate various connectivity scenarios and the different types of sediment transported, whether ash or soil. The event-scale parameterization of sediment transport could optimize peak prediction, as it takes into account the event differences.

## 4.2. OpenLISEM and MOHID Land performance

### 4.2.1. Quickflow and flow simulation

Calibration of event-based models is generally performed for each event separately, failing to obtain a good calibration with one calibration dataset (Baartman et al., 2012; Ebling et al., 2021; Rengers et al., 2016; Wu et al., 2021a). The current work presented a methodology that allows obtaining input hydrological parameter variation from event characteristics. This approach did not provide a single dataset, but created a consistent calibration dataset across events that incorporated temporal variability of (pre-event) conditions. Although the methodology allowed to derive input parameters for a wide range of rainfall events, it could imply a potential loss of efficiency compared with event-by-event calibration. However, choosing event-specific calibrations could lead to a disconnection between calibrated parameters across events, limiting the broader applicability of the method.

Both MOHID Land and OpenLISEM calibration revealed a good ability to simulate events characterized by a single peak using this methodology (Supplementary material Figure S1 and S3). Event h on the validation set was strongly overestimated by both models, probably due to the high maximum intensity of the rainfall event ( $67.2 \text{ mm hr}^{-1}$  compared to the average of  $24.9 \text{ mm hr}^{-1}$ ) making it an outlier compared to the events of the calibration set.

Several difficulties were also observed when simulating events characterized by two peak flows, with both models failing to simulate the presence of the first peak. The same difficulties were encountered by Vieira et al. (2022), with OpenLISEM failing to simulate peaks characterized by low intensity rainfall. The inability of either model to simulate the first peak may be due to the threshold behavior of runoff generation, in which certain conditions must be met before it begins. In the case of OpenLISEM, the threshold required to initiate surface runoff is probably not reached during low intensity rainfall, leading the model to fail to simulate the first peak (Jetten, 2018). A similar process occurs for MOHID Land, whereby losses due to evapotranspiration and infiltration overcome the formation of a water column (Trancoso et al., 2009). Unlike MOHID Land, in this study OpenLISEM was able to simulate the presence of multi peaks for higher intensities during the same event, likely because the model is sensitive to high intensity precipitation, responding quickly to it and leading to better simulation of peaks due to excess infiltration. From the events graphs in the Supplementary materials (Figure S1 and S2), it can be seen that OpenLISEM failed to reproduce the skewed nature of the hydrograph, affecting the performance of the model in predicting the overall total discharge. Nevertheless, OpenLISEM confirmed its validity to correctly estimate the peak flow and the time of the peaks, which are, arguably, more important for flood risk predictions than total discharge. The validation results confirmed the ability of the model to predict the time of the peak, but it overestimates the total and the peak discharge as also found by Vieira et al. (2022). The observed overestimation appears to result from inadequate parameterization of  $K_{sat}$  and Manning's  $n$  values due to conditions that deviate significantly from the range of events in the calibration dataset (event h – Figure S2) and the inability of the methodology to consider specific event characteristics (event k and l – Figure S2). On the other hand, MOHID Land generally simulated single peak flow rates better than OpenLISEM, except for event b (Supplementary material Figure S3) which was highly overestimated. Nevertheless, the shape of the modeled hydrographs resembled more the observations than the ones simulated with OpenLISEM, which was reflected in a better overall model performance in terms of total and peak discharge and time of the peaks.

When analyzing the validation events, MOHID Land confirmed to be a valid tool for the simulation of the hydrological response of the catchment. Although a slight worsening in simulating the time of the peak was visible, MOHID Land succeeded in better modeling the peak discharge and the total volume (Table 7 and Supplementary materials Figure S3 and S4). This improvement may be attributed to the model

consideration of subsurface flow. Incorporation of additional hydrologic processes could contribute to a more accurate simulation, potentially due to the lower sensitivity of the hydrologic response to parameters governing surface runoff. Prior research by Boulet et al. (2015) indicated that subsurface flow was the dominant process in the hydrological response for the Serra de Cima catchment before the fire. However, wildfires alter the infiltration capacity of the burned soils, affecting the post-fire hydrological response. Despite this alteration, subsurface flow can still play a crucial role in burned conditions, which could explain why MOHID Land better predicted peak volumes reaching the outlet of the watershed.

Nonetheless, it is essential to be cautious when relying only on model performance metrics, as they may drive the conclusion of the study (Clark et al., 2021). Therefore, the better performance of the MOHID Land model when compared to OpenLISEM for hydrological response can be explained by additional factors, such as model parametrization and model structure.

### 4.2.2. Sediment transport

The lack of sediment data and the scarcity of events made the sediment calibration and validation of both models difficult. Since the continuous values used for the analysis were derived from punctual ones collected by the autosampler during three rainfall events, their performance needs to be discussed cautiously.

Calibration and validation of both models revealed worse performance than Wu et al., (2021b), probably due to the lower erosion rate of the study area, which can be seen as a possible explanation for the difficulties in simulating sediment yield (Nearing, 2004). However, OpenLISEM performed better than Ebling et al. (2021), who modeled a similar total amount of sediment yield.

Achieving satisfactory performance is difficult when calibrating models at event scale. For these short time scales, the driving force of precipitation is the only one implemented in the model, thus neglecting the state of the system in terms of resistance to driving forces (Nearing, 2004).

Unlike OpenLISEM, MOHID Land model bases sediment transport processes on a wide range of equations, increasing thus the uncertainty in the predicted soil erosion (Parsons, 2019). As the model uses empirical functions to simulate sediment erosion and deposition, it was difficult to relate parameters to field measurements. Additionally, the limited literature availability on MOHID Land calibration for sediment transport has questioned whether the model correctly simulates or not erosion and deposition processes at hillslope scale. As a result of model overparameterization, MOHID Land predictions may be accurate for the wrong reasons due to equifinality caused by uncertainty in the calibration process (Batista et al., 2019). The authors of this work suggest that reducing the number of parameters in MOHID Land could decrease the dependence of parameter optimization on the calibrated area, and reduce the uncertainties in the modeling predictions. This could be made similarly to what is implemented in OpenLISEM, by including calibrated sediment transport equations directly in the model.

In light of the challenges encountered in performing event prediction, uncertainty analysis would strengthen the reliability of the results. An uncertainty analysis was executed for OpenLISEM hydrological response, assessing the variability of the results due to a 5 % variability on the calibrated parameters. The analysis revealed that the uncertainty is during the peak flow, with an average coefficient of variation of 15 %. Nevertheless, the elevated computational requirements restricted a similar analysis for MOHID Land model. In order not to create imbalances in the results and because the primary objective of the study was to develop and test a methodology for event-based model calibration, the OpenLISEM uncertainty analysis was not presented. In an operational setting of post-fire emergency prioritization and decision-making, uncertainty analysis is itself a necessity, simply because the prediction of rainfall events already has its share of uncertainties.

## 5. Conclusions

The main limitation of event-based models is their inability to obtain satisfactory model performance with a single set of values for the model input parameters. This is especially true for post-fire conditions due to the frequently rapid changes in vegetation and soil properties with time-since-fire. The findings of this study were the following:

- (i) A calibration approach was developed balancing between calibrated parameters and boundary conditions characterizing each event for two contrasting models.
- (ii) OpenLISEM and MOHID Land did not diverge markedly in their satisfactory capacity to simulate the runoff response at the outlet of a headwater catchment for selected rainfall events. While MOHID Land outperformed OpenLISEM in simulating the single-peak magnitude runoff events and total discharge better included in the validation data set, OpenLISEM stood out for its ease of implementation and its reduced computational requirements, always providing satisfactory results.
- (iii) OpenLISEM performed better in simulating the catchment's post-fire sediment yield produced by selected rainfall events. Parameterization of the erosion response was more uncertain in the case of MOHID Land, due to the larger number of underpinning equations and the greater discrepancy of the respective model input parameters from field measurements.
- (iv) OpenLISEM was preferred over MOHID Land, with smaller efforts involved in parameterizing and running the simulations and performing an uncertainty analysis. The ease of implementation of OpenLISEM outbalances the additional efforts involved in carrying out the required baseflow separation.

## CRedit authorship contribution statement

**Marta Basso:** Conceptualization, Methodology, Validation, Visualization, Writing – original draft, Writing – review & editing. **Jantiene Baartman:** Methodology, Writing – original draft, Writing – review & editing. **Martinho Martins:** Resources, Writing – review & editing. **Jacob Keizer:** Resources, Writing – original draft, Writing – review & editing. **Diana Vieira:** Conceptualization, Visualization, Writing – original draft, Writing – review & editing.

## Declaration of competing interest

The authors declare that they have no known competing financial interests or personal relationships that could have appeared to influence the work reported in this paper.

## Data availability

The authors do not have permission to share data.

## Acknowledgments

Thanks are due for the financial support from FCT– Fundação para a Ciência e a Tecnologia, I.P. and CESAM (UIDB/50017/2020+UIDP/50017/2020), through national funds. This work was supported by the projects ASHMOB (CENTRO-01-0145-FEDER-029351), FEMME (PCIF/MPG/0019/2017), and WAFLE (PTDC/ASP-SIL/31573/2017) funded by FEDER, through COMPETE2020 - Programa Operacional Competitividade e Internacionalização (POCI), and by national funds (OE), through FCT/MCTES, and by the project EPyRIS (SOE2/P5/E0811), funded by the European Union through the SUDOIE INTERREG Program. M. Basso was founded by FCT with an individual contract (SFRH/BD/146356/2019). We Thank CIRA for providing the digital terrain model (LICENÇA DE UTILIZAÇÃO n.º 1/CIRA/2020 pela Comunidade Inter-municipal da Região de Aveiro). Finally, we are most grateful to our

colleagues Sil van den Groenendael and Annelou Hoogerwerf for their help with the field data collection.

## Appendix A. Supplementary data

Supplementary data to this article can be found online at <https://doi.org/10.1016/j.jhydrol.2024.131258>.

## References

- APHA, 1998. Total suspended solids dried at 105 degrees Celsius method 2540D. In: Standard Methods for the Examination of Water and Waste Water. Washington, DC, USA.
- Arnold, J.G., Allen, P.M., Muttiah, R., Bernhardt, G., 1995. Automated base flow separation and recession analysis techniques. *Groundwater* 33, 1010–1018. <https://doi.org/10.1111/j.1745-6584.1995.tb00046.x>.
- Baartman, J.E.M., Jetten, V.G., Ritsema, C.J., de Vente, J., 2012. Exploring effects of rainfall intensity and duration on soil erosion at the catchment scale using openLISEM: Prado catchment, SE Spain. *Hydrol. Process.* 26, 1034–1049. <https://doi.org/10.1002/hyp.8196>.
- Baret, F., Guyot, G., Major, D.J., 1989. TSAVI: a vegetation index which minimizes soil brightness effects on LAI and APAR estimation.
- Baret, F., Guyot, G., 1991. Potentials and limits of vegetation indices for LAI and APAR assessment. *Remote Sens. Environ.* 35, 161–173. [https://doi.org/10.1016/0034-4257\(91\)90009-U](https://doi.org/10.1016/0034-4257(91)90009-U).
- Basso, M., Vieira, D.C.S., Ramos, T.B., Mateus, M., 2020. Assessing the adequacy of SWAT model to simulate postfire effects on the watershed hydrological regime and water quality. *L. Degrad. Dev.* 31, 619–631. <https://doi.org/10.1002/ldr.3476>.
- Basso, M., Serpa, D., Mateus, M., Keizer, J.J., Vieira, D.C.S., 2022a. Advances on water quality modeling in burned areas: a review. *PLOS Water* 1, e0000025.
- Basso, M., Serpa, D., Rocha, J., Martins, M.A.S., Keizer, J., Vieira, D.C.S., 2022b. A modelling approach to evaluate land management options for recently burnt catchments. *Eur. J. Soil Sci.* 73, e13275.
- Batista, P.V.G., Davies, J., Silva, M.L.N., Quinton, J.N., 2019. On the evaluation of soil erosion models: Are we doing enough? *Earth-Science Rev.* 197, 102898 <https://doi.org/10.1016/j.earscirev.2019.102898>.
- Bladon, K.D., Emelko, M.B., Silins, U., Stone, M., 2014. Wildfire and the Future of Water Supply. *Environ. Sci. Technol.* 48, 8936–8943. <https://doi.org/10.1021/es500130g>.
- Boulet, A.-K., Prats, S.A., Malvar, M.C., González-Pelayo, O., Coelho, C.O.A., Ferreira, A. J.D., Keizer, J.J., 2015. Surface and subsurface flow in eucalyptus plantations in north-central Portugal. *J. Hydrol. Hydromechanics* 63, 193–200.
- Boulet, A.-K., Rial-Rivas, M.E., Ferreira, C., Coelho, C.O.A., Kalantari, Z., Keizer, J.J., Ferreira, A.J.D., 2021. Hydrological Processes in Eucalypt and Pine Forested Headwater Catchments within Mediterranean Region. *Water*. <https://doi.org/10.3390/w13101418>.
- Breda, N.J.J., 2003. Ground-based measurements of leaf area index: a review of methods, instruments and current controversies. *J. Exp. Bot.* 54, 2403–2417.
- Brito, D., Ramos, T.B., Gonçalves, M.C., Morais, M., Neves, R., 2018. Integrated modelling for water quality management in a eutrophic reservoir in south-eastern Portugal. *Environ. Earth Sci.* 77, 40. <https://doi.org/10.1007/s12665-017-7221-5>.
- Campos, I., Abrantes, N., Vidal, T., Bastos, A.C., Gonçalves, F., Keizer, J.J., 2012. Assessment of the toxicity of ash-loaded runoff from a recently burnt eucalypt plantation. *Eur. J. for. Res.* 131, 1889–1903. <https://doi.org/10.1007/s10342-012-0640-7>.
- Canfield, H.E., Goodrich, D.C., Burns, I.S., 2005. Selection of parameters values to model post-fire runoff and sediment transport at the watershed scale in southwestern forests. *Managing Watersheds for Human and Natural Impacts: Engineering, Ecological, and Economic Challenges*. 1–12. [https://doi.org/10.1061/40763\(178\)48](https://doi.org/10.1061/40763(178)48).
- Cannon, S.H., Gartner, J.E., Wilson, R.C., Bowers, J.C., Laber, J.L., 2008. Storm rainfall conditions for floods and debris flows from recently burned areas in southwestern Colorado and southern California. *Geomorphology* 96, 250–269. <https://doi.org/10.1016/j.geomorph.2007.03.019>.
- Cerdà, A., 1998. Changes in overland flow and infiltration after a rangeland fire in a Mediterranean scrubland. *Hydrol. Process.* 12, 1031–1042. [https://doi.org/10.1002/\(SICI\)1099-1085\(19980615\)12:7<1031::AID-HYP636>3.0.CO;2-V](https://doi.org/10.1002/(SICI)1099-1085(19980615)12:7<1031::AID-HYP636>3.0.CO;2-V).
- Chen, L., Berli, M., Chief, K., 2013. Examining modeling approaches for the rainfall-runoff process in wildfire-affected watersheds: Using San Dimas Experimental Forest. *JAWRA J. Am. Water Resour. Assoc.* 49, 851–866. <https://doi.org/10.1111/jawr.12043>.
- Clark, M.P., Vogel, R.M., Lamontagne, J.R., Mizukami, N., Knoben, W.J.M., Tang, G., Gharari, S., Freer, J.E., Whitfield, P.H., Shook, K.R., Papalexioiu, S.M., 2021. The Abuse of Popular Performance Metrics in Hydrologic Modeling. *e2020WR029001 Water Resour. Res.* 57. <https://doi.org/10.1029/2020WR029001>.
- Coelho, C., Shakesby, R.A., Walsh, R.P.D., 1995. Effects of Forest Fires and Post-fire Land Management Practice on Soil Erosion and Stream Dynamics, Águeda Basin, Portugal: Soil and Groundwater Research Report V. European commission, Luxembourg.
- De Girolamo, A.M., Cerdan, O., Grangeon, T., Ricci, G.F., Vandromme, R., Lo Porto, A., 2022. Modelling effects of forest fire and post-fire management in a catchment prone to erosion: Impacts on sediment yield. *CATENA* 212, 106080. <https://doi.org/10.1016/j.catena.2022.106080>.
- De Roo, A.P.J., Offermans, R.J.E., Cremens, N.H.D.T., 1996a. LISEM: A single-event physically based hydrological and soil erosion model for drainage basins. II:

- Sensitivity analysis, validation and application. *Hydrol. Process.* 10, 1119–1126. [https://doi.org/10.1002/\(SICI\)1099-1085\(199608\)10:8<1119::AID-HYP416>3.0.CO;2-V](https://doi.org/10.1002/(SICI)1099-1085(199608)10:8<1119::AID-HYP416>3.0.CO;2-V).
- De Roo, A.P.J., Wesseling, C.G., Ritsema, C.J., 1996b. LISEM: A single-event physically based hydrological and soil erosion model for drainage basins. I. Theory, input and output. *Hydrol. Process.* 10, 1107–1117. [https://doi.org/10.1002/\(SICI\)1099-1085\(199608\)10:8<1107::AID-HYP415>3.0.CO;2-4](https://doi.org/10.1002/(SICI)1099-1085(199608)10:8<1107::AID-HYP415>3.0.CO;2-4).
- Doerr, S.H., Thomas, A.D., 2000. The role of soil moisture in controlling water repellency: new evidence from forest soils in Portugal. *J. Hydrol.* 231–232, 134–147. [https://doi.org/10.1016/S0022-1694\(00\)00190-6](https://doi.org/10.1016/S0022-1694(00)00190-6).
- Ebel, B.A., 2019. Measurement method has a larger impact than spatial scale for plot-scale field-saturated hydraulic conductivity (Kfs) after wildfire and prescribed fire in forests. *Earth Surf. Process. Landforms* 44, 1945–1956. <https://doi.org/10.1002/esp.4621>.
- Ebel, B.A., Martin, D.A., 2017. Meta-analysis of field-saturated hydraulic conductivity recovery following wildland fire: Applications for hydrologic model parameterization and resilience assessment. *Hydrol. Process.* 31, 3682–3696. <https://doi.org/10.1002/hyp.11288>.
- Ebel, B.A., Moody, J.A., 2020. Parameter estimation for multiple post-wildfire hydrologic models. *Hydrol. Process.* 34, 4049–4066. <https://doi.org/10.1002/hyp.13865>.
- Ebling, É.D., Reichert, J.M., Zuluaga Peláez, J.J., Rodrigues, M.F., Valente, M.L., Lopes Cavalcante, R.B., Reggiani, P., Srinivasan, R., 2021. Event-based hydrology and sedimentation in paired watersheds under commercial eucalyptus and grasslands in the Brazilian Pampa biome. *Int. Soil Water Conserv. Res.* 9, 180–194. <https://doi.org/10.1016/j.iswcr.2020.10.008>.
- Emelko, M.B., Silins, U., Bladon, K.D., Stone, M., 2011. Implications of land disturbance on drinking water treatability in a changing climate: Demonstrating the need for “source water supply and protection” strategies. *Water Res.* 45, 461–472. <https://doi.org/10.1016/j.watres.2010.08.051>.
- Fernández, C., Vega, J.A., 2016. Evaluation of RUSLE and PESERA models for predicting soil erosion losses in the first year after wildfire in NW Spain. *Geoderma* 273, 64–72. <https://doi.org/10.1016/j.geoderma.2016.03.016>.
- Ferreira, A.J.D., Coelho, C.O.A., Walsh, R.P.D., Shakesby, R.A., Ceballos, A., Doerr, S.H., 2000. Hydrological implications of soil water-repellency in Eucalyptus globulus forests, north-central Portugal. *J. Hydrol.* 231–232, 165–177. [https://doi.org/10.1016/S0022-1694\(00\)00192-X](https://doi.org/10.1016/S0022-1694(00)00192-X).
- Girona-García, A., Vieira, D.C.S., Silva, J., Fernández, C., Robichaud, P.R., Keizer, J.J., 2021. Effectiveness of post-fire soil erosion mitigation treatments: A systematic review and meta-analysis. *Earth-Science Rev.* 103611 <https://doi.org/10.1016/j.earscirev.2021.103611>.
- Gupta, H.V., Kling, H., Yilmaz, K.K., Martinez, G.F., 2009. Decomposition of the mean squared error and NSE performance criteria: Implications for improving hydrological modelling. *J. Hydrol.* 377, 80–91. <https://doi.org/10.1016/j.jhydrol.2009.08.003>.
- Havel, A., Tasdighi, A., Arabi, M., 2018. Assessing the hydrologic response to wildfires in mountainous regions. *Hydrol. Earth Syst. Sci.* 22, 2527–2550. <https://doi.org/10.5194/hess-22-2527-2018>.
- Iooss, B., Janon, A., Pujol, G., Broto, B., Boumhaout, K., Da Veiga, S., Delage, T., Fruth, J., Gilquin, L., Guillaume, J., 2021. Sensitivity: global sensitivity analysis of model outputs. R Packag. version 1.
- Jetten, V., 2018. OpenLISEM. Multi-Hazard Land Surface Process Model. Documentation & User Manual.
- Keeley, J.E., 2009. Fire intensity, fire severity and burn severity: a brief review and suggested usage. *Int. J. Wildl. Fire* 18, 116–126. <https://doi.org/10.1071/WF07049>.
- Keizer, J.J., Doerr, S.H., Malvar, M.C., Prats, S.A., Ferreira, R.S.V., Oñate, M.G., Coelho, C.O.A., Ferreira, A.J.D., 2008. Temporal variation in topsoil water repellency in two recently burnt eucalypt stands in north-central Portugal. *CATENA* 74, 192–204. <https://doi.org/10.1016/j.catena.2008.01.004>.
- Knoben, W.J.M., Freer, J.E., Woods, R.A., 2019. Technical note: Inherent benchmark or not? Comparing Nash-Sutcliffe and Kling-Gupta efficiency scores. *Hydrol. Earth Syst. Sci.* 23, 4323–4331. <https://doi.org/10.5194/hess-23-4323-2019>.
- Krause, P., Boyle, D.P., Bäse, F., 2005. Comparison of different efficiency criteria for hydrological model assessment. *Adv. Geosci.* 5, 89–97. <https://doi.org/10.5194/adgeo-5-89-2005>.
- Kutiel, P., Lavee, H., Segev, M., Benyamini, Y., 1995. The effect of fire-induced surface heterogeneity on rainfall-runoff-erosion relationships in an eastern Mediterranean ecosystem, Israel. *CATENA* 25, 77–87. [https://doi.org/10.1016/0341-8162\(94\)00043-E](https://doi.org/10.1016/0341-8162(94)00043-E).
- Larsen, L.J., MacDonald, L.H., 2007. Predicting postfire sediment yields at the hillslope scale: Testing RUSLE and Disturbed WEPP. *Water Resour. Res.* 43 <https://doi.org/10.1029/2006WR005560>.
- Leighton-Boyce, G., Doerr, S.H., Shakesby, R.A., Walsh, R.P.D., Ferreira, A.J.D., Boulet, A.-K., Coelho, C.O.A., 2005. Temporal dynamics of water repellency and soil moisture in eucalypt plantations. *Portugal. Soil Res.* 43, 269–280.
- Liu, T., McGuire, L.A., Wei, H., Rengers, F.K., Gupta, H., Ji, L., Goodrich, D.C., 2021. The timing and magnitude of changes to Hortonian overland flow at the watershed scale during the post-fire recovery process. *Hydrol. Process.* 35, e14208.
- Lopes, A.R., Girona-García, A., Corticeiro, S., Martins, R., Keizer, J.J., Vieira, D.C.S., 2021. What is wrong with post-fire soil erosion modelling? A meta-analysis on current approaches, research gaps, and future directions. *Earth Surf. Process. Landforms* 46, 205–219. <https://doi.org/10.1002/esp.5020>.
- Lutes, D.C., Keane, R.E., Caratti, J.F., Key, C.H., Benson, N.C., Sutherland, S., Gangi, L.J., 2006. FIREMON: Fire effects monitoring and inventory system. Fort Collins, CO: U.S. Department of Agriculture, Forest Service, Rocky Mountain Research Station. 1 CD.
- Madeira, M.A.V., 1989. In: *Changes in Soil Properties under Eucalyptus Plantations in Portugal BT - Biomass Production by Fast-Growing Trees*. Springer, Netherlands, Dordrecht, pp. 81–99. [https://doi.org/10.1007/978-94-009-2348-5\\_6](https://doi.org/10.1007/978-94-009-2348-5_6).
- Martins, M.A.S., Machado, A.I., Serpa, D., Prats, S.A., Faria, S.R., Varela, M.E.T., González-Pelayo, Ó., Keizer, J.J., 2013. Runoff and inter-rill erosion in a Maritime Pine and a Eucalypt plantation following wildfire and terracing in north-central Portugal. *J. Hydrol. Hydromechanics* 61, 261–268. <https://doi.org/10.2478/johh-2013-0033>.
- Mataix-Solera, J., Cerdà, A., Arcenegui, V., Jordán, A., Zavala, L.M., 2011. Fire effects on soil aggregation: A review. *Earth-Science Rev.* 109, 44–60. <https://doi.org/10.1016/j.earscirev.2011.08.002>.
- Moody, J.A., Kinner, D.A., 2006. Spatial structures of stream and hillslope drainage networks following gully erosion after wildfire. *Earth Surf. Process. Landforms* 31, 319–337. <https://doi.org/10.1002/esp.1246>.
- Moody, J.A., Smith, J.D., Ragan, B.W., 2005. Critical shear stress for erosion of cohesive soils subjected to temperatures typical of wildfires. *J. Geophys. Res. Earth Surf.* 110 <https://doi.org/10.1029/2004JF000141>.
- Moody, J.A., Shakesby, R.A., Robichaud, P.R., Cannon, S.H., Martin, D.A., 2013. Current research issues related to post-wildfire runoff and erosion processes. *Earth-Science Rev.* 122, 10–37. <https://doi.org/10.1016/j.earscirev.2013.03.004>.
- Morgan, R.P.C., 2001. A simple approach to soil loss prediction: a revised Morgan–Morgan–Finney model. *CATENA* 44, 305–322. [https://doi.org/10.1016/S0341-8162\(00\)00171-5](https://doi.org/10.1016/S0341-8162(00)00171-5).
- Moriassi, D.N., Gitau, M.W., Pai, N., Daggupati, P., 2015. Hydrologic and water quality models: Performance measures and evaluation criteria. *Trans. ASABE* 58, 1763–1785. <https://doi.org/10.13031/trans.58.10715>.
- Moussoulis, E., Mallinis, G., Koutsias, N., Zacharias, I., 2015. Modelling surface runoff to evaluate the effects of wildfires in multiple semi-arid, shrubland-dominated catchments. *Hydrol. Process.* 29, 4427–4441. <https://doi.org/10.1002/hyp.10509>.
- Mualem, Y., 1976. A new model for predicting the hydraulic conductivity of unsaturated porous media. *Water Resour. Res.* 12, 513–522. <https://doi.org/10.1029/WR012i003p00513>.
- Murphy, B.P., Czuba, J.A., Belmont, P., 2019. Post-wildfire sediment cascades: A modeling framework linking debris flow generation and network-scale sediment routing. *Earth Surf. Process. Landforms* 44, 2126–2140. <https://doi.org/10.1002/esp.4635>.
- Murphy, S.F., Writer, J.H., McCleskey, R.B., Martin, D.A., 2015. The role of precipitation type, intensity, and spatial distribution in source water quality after wildfire. *Environ. Res. Lett.* 10, 84007. <https://doi.org/10.1088/1748-9326/10/8/084007>.
- Nearing, M.A., 2004. Capabilities and limitations of erosion models and data. In: *Proceedings of the 13th International Soil Conservation Organization Conference*, pp. 4–8.
- Neary, D.G., Gottfried, G.J., 2002. Fires and floods: post-fire watershed responses., in: *Forest Fire Research and Wildland Fire Safety: Proceedings of IV International Conference on Forest Fire Research 2002 Wildland Fire Safety Summit*, Luso, Coimbra, Portugal, 18–23 November 2002. Millpress Science Publishers.
- Nunes, J.P., Doerr, S.H., Sheridan, G., Neris, J., Santín Nuño, C., Emelko, M.B., Silins, U., Robichaud, P.R., Elliot, W.J., Keizer, J., 2018a. Assessing water contamination risk from vegetation fires: Challenges, opportunities and a framework for progress. *Hydrol. Process.* <https://doi.org/10.1002/hyp.11434>.
- Nunes, J.P., Naranjo Quintanilla, P., Santos, J.M., Serpa, D., Carvalho-Santos, C., Rocha, J., Keizer, J.J., Keesstra, S.D., 2018b. Afforestation, Subsequent Forest Fires and Provision of Hydrological Services: A Model-Based Analysis for a Mediterranean Mountainous Catchment. *L. Degrad. Dev.* 29, 776–788. <https://doi.org/10.1002/ldr.2776>.
- Parsons, A.J., 2019. How reliable are our methods for estimating soil erosion by water? *Sci. Total Environ.* 676, 215–221. <https://doi.org/10.1016/j.scitotenv.2019.04.307>.
- Pereira, P., Cerdà, A., Úbeda, X., Mataix-Solera, J., Arcenegui, V., Zavala, L.M., 2015. Modelling the Impacts of Wildfire on Ash Thickness in a Short-Term Period. *L. Degrad. Dev.* 26, 180–192. <https://doi.org/10.1002/ldr.2195>.
- Pereira, V., FitzPatrick, E.A., 1995. Cambisols and related soils in north-central Portugal: their genesis and classification. *Geoderma* 66, 185–212. [https://doi.org/10.1016/0016-7061\(94\)00076-M](https://doi.org/10.1016/0016-7061(94)00076-M).
- Qi, J., Chehbouni, A., Huete, A.R., Kerr, Y.H., Sorooshian, S., 1994. A modified soil adjusted vegetation index. *Remote Sens. Environ.* 48, 119–126. [https://doi.org/10.1016/0034-4257\(94\)90134-1](https://doi.org/10.1016/0034-4257(94)90134-1).
- Qi, J., Marslett, R.C., Moran, M.S., Goodrich, D.C., Heilman, P., Kerr, Y.H., Dedieu, G., Chehbouni, A., Zhang, X.X., 2000. Spatial and temporal dynamics of vegetation in the San Pedro River basin area. *Agric. for. Meteorol.* 105, 55–68. [https://doi.org/10.1016/S0168-1923\(00\)00195-7](https://doi.org/10.1016/S0168-1923(00)00195-7).
- Rawls, J.W., Brakensiek, L.D., Miller, N., 1983. Green-ampt Infiltration Parameters from Soils Data. *J. Hydraul. Eng.* 109, 62–70. [https://doi.org/10.1061/\(ASCE\)0733-9429\(1983\)109:1\(62\)](https://doi.org/10.1061/(ASCE)0733-9429(1983)109:1(62)).
- Renard, K.G., Foster, G.R., Weesies, G.A., Porter, J.P., 1991. RUSLE: Revised universal soil loss equation. *J. Soil Water Conserv.* 46, 30–33.
- Rengers, F.K., McGuire, L.A., Kean, J.W., Staley, D.M., Hobley, D.E.J., 2016. Model simulations of flood and debris flow timing in steep catchments after wildfire. *Water Resour. Res.* 52, 6041–6061. <https://doi.org/10.1002/2015WR018176>.
- Robichaud, P.R., 2000. Fire effects on infiltration rates after prescribed fire in Northern Rocky Mountain forests. *USA. J. Hydrol.* 231, 220–229. [https://doi.org/10.1016/S0022-1694\(00\)00196-7](https://doi.org/10.1016/S0022-1694(00)00196-7).
- Robichaud, P.R., Elliot, W.J., Pierson, F.B., Hall, D.E., Moffet, C.A., 2007. Predicting postfire erosion and mitigation effectiveness with a web-based probabilistic erosion model. *CATENA* 71, 229–241. <https://doi.org/10.1016/j.catena.2007.03.003>.
- Rulli, M.C., Rosso, R., 2005. Modeling catchment erosion after wildfires in the San Gabriel Mountains of southern California. *Geophys. Res. Lett.* 32 <https://doi.org/10.1029/2005GL023635>.

- Rulli, M.C., Offeddu, L., Santini, M., 2013. Modeling post-fire water erosion mitigation strategies. *Hydrol. Earth Syst. Sci.* 17, 2323–2337. <https://doi.org/10.5194/hess-17-2323-2013>.
- Rulli, M.C., Rosso, R., 2007. Hydrologic response of upland catchments to wildfires. *Adv. Water Resour.* 30, 2072–2086. <https://doi.org/10.1016/j.advwatres.2006.10.012>.
- Santos, J.M., Verheijen, F.G.A., Tavares Wahren, F., Wahren, A., Feger, K.-H., Bernard-Jannin, L., Rial-Rivas, M.E., Keizer, J.J., Nunes, J.P., 2016. Soil Water Repellency Dynamics in Pine and Eucalypt Plantations in Portugal. *A High-resolution Time Series. L. Degrad. Dev.* 27, 1334–1343. <https://doi.org/10.1002/ldr.2251>.
- Shakesby, R.A., 2011. Post-wildfire soil erosion in the Mediterranean: Review and future research directions. *Earth-Science Rev.* 105, 71–100. <https://doi.org/10.1016/j.earscirev.2011.01.001>.
- Shakesby, R.A., Boakes, D.J., de OA Coelho, C., Gonçalves, A.J.B., Walsh, R.P.D., 1996. Limiting the soil degradational impacts of wildfire in pine and eucalyptus forests in Portugal: a comparison of alternative post-fire management practices. *Appl. Geogr.* 16, 337–355.
- Shakesby, R.A., Doerr, S.H., 2006. Wildfire as a hydrological and geomorphological agent. *Earth-Science Rev.* 74, 269–307. <https://doi.org/10.1016/j.earscirev.2005.10.006>.
- Smith, H.G., Sheridan, G.J., Lane, P.N.J., Nyman, P., Haydon, S., 2011. Wildfire effects on water quality in forest catchments: A review with implications for water supply. *J. Hydrol.* 396, 170–192. <https://doi.org/10.1016/j.jhydrol.2010.10.043>.
- SNIRH, 2020. Serviço Nacional de Informação sobre Recursos Hídricos [WWW Document]. URL <https://snirh.apambiente.pt/> (accessed 10.11.20).
- Sobol', I.M., 1990. On sensitivity estimation for nonlinear mathematical models. *Mat. Model.* 2, 112–118.
- Srivastava, A., Wu, J.Q., Elliot, W.J., Brooks, E.S., Flanagan, D.C., 2018. A simulation study to estimate effects of wildfire and forest management on hydrology and sediment in a Forested Watershed, Northwestern U.S. *Trans. ASABE* 61, 1579–1601. <https://doi.org/10.13031/trans.12326>.
- Strahler, A.N., 1957. Quantitative analysis of watershed geomorphology. *Eos Trans. Am. Geophys. Union* 38, 913–920.
- Thomas, G., Rosalie, V., Olivier, C., Anna Maria, D.G., Antonio, L.P., 2021. Modelling forest fire and firebreak scenarios in a mediterranean mountainous catchment: Impacts on sediment loads. *J. Environ. Manage.* 289, 112497 <https://doi.org/10.1016/j.jenvman.2021.112497>.
- Trancoso, A.R., Braunschweig, F., Leitão, P.C., Obermann, M., Neves, R., 2009. An advanced modelling tool for simulating complex river systems. *Sci. Total Environ.* 407, 3004–3016.
- van Dijk, A.I.J., Bruijnzeel, L.A., Rosewell, C.J., 2002. Rainfall intensity–kinetic energy relationships: a critical literature appraisal. *J. Hydrol.* 261, 1–23. [https://doi.org/10.1016/S0022-1694\(02\)00020-3](https://doi.org/10.1016/S0022-1694(02)00020-3).
- Van Eck, C.M., Nunes, J.P., Vieira, D.C.S., Keesstra, S., Keizer, J.J., 2016. Physically-based modelling of the post-fire runoff response of a forest catchment in Central Portugal: using field versus remote sensing based estimates of vegetation recovery. *L. Degrad. Dev.* 27, 1535–1544. <https://doi.org/10.1002/ldr.2507>.
- van Genuchten, M.T., 1980. A closed-form equation for predicting the hydraulic conductivity of unsaturated soils. *Soil Sci. Soc. Am. J.* 44, 892–898. <https://doi.org/10.2136/sssaj1980.03615995004400050002x>.
- Vieira, D.C.S., Prats, S.A., Nunes, J.P., Shakesby, R.A., Coelho, C.O.A., Keizer, J.J., 2014. Modelling runoff and erosion, and their mitigation, in burned Portuguese forest using the revised Morgan–Morgan–Finney model. *For. Ecol. Manage.* 314, 150–165. <https://doi.org/10.1016/j.foreco.2013.12.006>.
- Vieira, D.C.S., Fernández, C., Vega, J.A., Keizer, J.J., 2015. Does soil burn severity affect the post-fire runoff and interrill erosion response? A review based on meta-analysis of field rainfall simulation data. *J. Hydrol.* 523, 452–464. <https://doi.org/10.1016/j.jhydrol.2015.01.071>.
- Vieira, D.C.S., Malvar, M.C., Martins, M.A.S., Serpa, D., Keizer, J.J., 2018a. Key factors controlling the post-fire hydrological and erosive response at micro-plot scale in a recently burned Mediterranean forest. *Geomorphology* 319, 161–173. <https://doi.org/10.1016/j.geomorph.2018.07.014>.
- Vieira, D.C.S., Serpa, D., Nunes, J.P.C., Prats, S.A., Neves, R., Keizer, J.J., 2018b. Predicting the effectiveness of different mulching techniques in reducing post-fire runoff and erosion at plot scale with the RUSLE, MMF and PESERA models. *Environ. Res.* 165, 365–378. <https://doi.org/10.1016/j.envres.2018.04.029>.
- Vieira, D.C.S., Basso, M., Nunes, J.P., Keizer, J.J., Baartman, J.E.M., 2022. Event-based quickflow simulation with OpenLISEM in a burned Mediterranean forest catchment. *Int. J. Wildl. Fire.*
- Wagenbrenner, J.W., Ebel, B.A., Bladon, K.D., Kinoshita, A.M., 2021. Post-wildfire hydrologic recovery in Mediterranean climates: A systematic review and case study to identify current knowledge and opportunities. *J. Hydrol.* 602, 126772 <https://doi.org/10.1016/j.jhydrol.2021.126772>.
- Wu, J., Baartman, J.E.M., Nunes, J.P., 2021a. Testing the impacts of wildfire on hydrological and sediment response using the OpenLISEM model. Part 2: Analyzing the effects of storm return period and extreme events. *CATENA* 207, 105620. <https://doi.org/10.1016/j.catena.2021.105620>.
- Wu, J., Nunes, J.P., Baartman, J.E.M., Faúndez Urbina, C.A., 2021b. Testing the impacts of wildfire on hydrological and sediment response using the OpenLISEM model. Part 1: Calibration and evaluation for a burned Mediterranean forest catchment. *CATENA* 207, 105658. <https://doi.org/10.1016/j.catena.2021.105658>.
- Zanke, U., 1977. Berechnung der Sinkgeschwindigkeiten von Sedimenten.